SARS-CoV-2 infection and persistence throughout the human body and brain

Daniel Chertow (chertowd@cc.nih.gov)
National Institutes of Health https://orcid.org/0000-0002-1675-1728

Sydney Stein
National Institutes of Health https://orcid.org/0000-0002-0259-4485

Sabrina Ramelli
National Institutes of Health

Alison Grazioli
National Institutes of Health

Joon-Yong Chung
NCI https://orcid.org/0000-0001-5041-5982

Manmeet Singh
National Institutes of Health

Claude Kwe Yinda
National Institute of Allergy and Infectious Diseases

Clayton Winkler
National Institutes of Health

James Dickey
National Institutes of Health

Kris Ylaya
National Cancer Institute

Sung Hee Ko
National Institutes of Health

Andrew Platt
National Institutes of Health

Peter Burbelo
8Dental Clinical Research Core, NIDCR, NIH https://orcid.org/0000-0003-1717-048X

Martha Quezado
National Institutes of Health

Stefania Pittaluga
NIH

Madeleine Purcell
University of Maryland School of Medicine

Vincent Munster

National Institute of Allergy and Infectious Diseases https://orcid.org/0000-0002-2288-3196
Frida Belinky
NIH
Marcos Ramos-Benitez
National Institutes of Health
Eli Boritz
National Institutes of Health
Daniel Herr
University of Maryland School of Medicine
Joseph Rabin
University of Maryland School of Medicine
Kapil Saharia
University of Maryland School of Medicine
Ronson Madathil
University of Maryland School of Medicine
Ali Tabatabai
University of Maryland School of Medicine
Shahabuddin Soherwardi
TidalHealth Peninsula Regional
Michael McCurdy
University of Maryland St. Joseph Medical Center https://orcid.org/0000-0001-5319-0475
Karin Peterson
National Institutes of Health
Jeffrey Cohen
National Institutes of Health
Emmie de Wit
National Institute of Allergy and Infectious Diseases https://orcid.org/0000-0002-9763-7758
Kevin Vannella
National Institutes of Health
Stephen Hewitt
National Cancer Institute, National Institutes of Health https://orcid.org/0000-0001-8283-1788
David Kleiner
National Cancer Institute https://orcid.org/0000-0003-3442-4453

Biological Sciences - Article

Keywords:

Posted Date: December 20th, 2021

DOI: https://doi.org/10.21203/rs.3.rs-1139035/v1

SARS-CoV-2 infection and persistence throughout the human body and brain

Authors:

Sydney R. Stein[1,2], Sabrina C. Ramelli[3], Alison Grazioli[4], Joon-Yong Chung[5], Manmeet Singh[6], Claude Kwe Yinda[6], Clayton W. Winkler[7], James M. Dickey[1,2], Kris Ylaya[5], Sung Hee Ko[8], Andrew Platt[1,2], Peter D. Burbelo[9], Martha Quezado[5], Stefania Pittaluga[5], Madeleine Purcell[10], Vincent J. Munster[6], Frida Belinky[8], Marcos J. Ramos-Benitez[1,2,11], Eli A. Boritz[8], Daniel L. Herr[12], Joseph Rabin[13], Kapil K. Saharia[14,15], Ronson J. Madathil[16], Ali Tabatabai[17], Shahabuddin Soherwardi[18], Michael T. McCurdy[19,17], NIH COVID-19 Autopsy Consortium^, Karin E. Peterson[7], Jeffrey I. Cohen[19], Emmie de Wit[6], Kevin M. Vannella[1,2], Stephen M. Hewitt[5], David E. Kleiner[5], Daniel S. Chertow[1,2*]

Affiliations:

1. Emerging Pathogens Section, Critical Care Medicine Department, Clinical Center, National Institutes of Health, Bethesda, MD, USA
2. Laboratory of Immunoregulation, National Institute of Allergy and Infectious Diseases, National Institutes of Health, Bethesda, MD, USA
3. Critical Care Medicine Department, Clinical Center, National Institutes of Health, Bethesda, MD, USA
4. Kidney Disease Section, Kidney Diseases Branch, National Institute of Diabetes and Digestive and Kidney Diseases, National Institutes of Health, Bethesda, MD, USA
5. Laboratory of Pathology, Center for Cancer Research, National Cancer Institute, National Institutes of Health, Bethesda, MD, USA

6. Laboratory of Virology, Division of Intramural Research, National Institute of Allergy and Infectious Diseases, National Institute of Health, Hamilton, MT, USA
7. Laboratory of Persistence Viral Diseases, Rocky Mountain Laboratories, National Institute of Allergy and Infectious Diseases, National Institute of Health, Hamilton, MT, USA
8. Vaccine Research Center, National Institute of Allergy and Infectious Diseases, National Institutes of Health, Bethesda, MD, USA
9. National Institute of Dental and Craniofacial Research, National Institutes of Health, Bethesda, MD, USA
10. University of Maryland School of Medicine, Baltimore, MD, USA
11. Postdoctoral Research Associate Training Program, National Institute of General Medical Sciences, National Institutes of Health, Bethesda, MD, USA
12. R Adams Cowley Shock Trauma Center, Department of Medicine and Program in Trauma, University of Maryland School of Medicine, Baltimore, MD, USA
13. R Adams Cowley Shock Trauma Center, Department of Surgery and Program in Trauma, University of Maryland School of Medicine, Baltimore, MD, USA
14. Department of Medicine, Division of Infectious Disease, University of Maryland School of Medicine, Baltimore, MD, USA
15. Institute of Human Virology, University of Maryland School of Medicine, Baltimore, MD, USA
16. Department of Surgery, Division of Cardiac Surgery, University of Maryland School of Medicine, Baltimore, MD, USA

17. Department of Medicine, Division of Pulmonary and Critical Care Medicine, University of Maryland School of Medicine, Baltimore, MD, USA
18. Hospitalist Department, TidalHealth Peninsula Regional, Salisbury, MD, USA
19. Division of Critical Care Medicine, Department of Medicine, University of Maryland St. Joseph Medical Center, Towson, MD, USA
20. Medical Virology Section, Laboratory of Infectious Diseases, National Institute of Allergy and Infectious Diseases, National Institutes of Health, Bethesda MD
^See Acknowledgements
*Corresponding author. Email: chertowd@cc.nih.gov

COVID-19 is known to cause multi-organ dysfunction[1-3] in acute infection, with prolonged symptoms experienced by some patients, termed Post-Acute Sequelae of SARS-CoV-2 (PASC)[4-5]. However, the burden of infection outside the respiratory tract and time to viral clearance is not well characterized, particularly in the brain[3,6-14]. We performed complete autopsies on 44 patients with COVID-19 to map and quantify SARS-CoV-2 distribution, replication, and cell-type specificity across the human body, including brain, from acute infection through over seven months following symptom onset. We show that SARS-CoV-2 is widely distributed, even among patients who died with asymptomatic to mild COVID-19, and that virus replication is present in multiple pulmonary and extrapulmonary tissues early in infection. Further, we detected persistent SARS-CoV-2 RNA in multiple anatomic sites, including regions throughout the brain, for up to 230 days following symptom onset. Despite extensive distribution of SARS-CoV-2 in the body, we observed a paucity of inflammation or direct viral cytopathology outside of the lungs. Our data prove that SARS-CoV-2 causes systemic infection and can persist in the body for months.

Main text:

Infection with severe acute respiratory syndrome coronavirus 2 (SARS-CoV-2), the causative agent of coronavirus disease 2019 (COVID-19), has well described pulmonary and extrapulmonary manifestations[1-3], including multiorgan failure and shock among severe and fatal cases. Some survivors experience Post-Acute Sequelae of SARS-CoV-2 (PASC) – also known as Long COVID—with cardiovascular, pulmonary, and neurological manifestations with or without functional impairment[4-5]. While autopsy studies of fatal COVID-19 cases support the ability of SARS-CoV-2 to infect multiple organs[3,7-12], extra-pulmonary organs often lack histopathological

evidence of direct virally-mediated injury or inflammation[10-14]. The paradox of extra-pulmonary infection without injury or inflammation raises many pathogen- and host-related questions. These questions include, but are not limited to: What is the burden of infection within versus outside of the respiratory tract? What cell types are infected across extra-pulmonary tissues, and do they support SARS-CoV-2 infection and replication? In the absence of cellular injury and inflammation in extra-pulmonary tissues, does SARS-CoV-2 persist, and if so, over what interval? Does SARS-CoV-2 evolve as it spreads to and persists in different anatomical compartments?

To inform these pathogen-focused questions and to evaluate for the presence or absence of associated histopathology in matched tissue specimens, we performed extensive autopsies on a diverse population of 44 individuals who died from or with COVID-19 up to 230 days following initial symptom onset. Our approach focused on timely, systematic, and comprehensive tissue sampling and preservation of adjacent tissue samples for complementary analyses. We performed droplet digital polymerase chain reaction (ddPCR) for sensitive detection and quantification of SARS-CoV-2 gene targets in all tissue samples collected. To elucidate SARS-CoV-2 cell-type specificity and validate ddPCR findings, we performed *in situ* hybridization (ISH) broadly across sampled tissues. Immunohistochemistry (IHC) was used to further validate cell-type specificity in the brain where controversy remains on the regional distribution and cellular tropism of SARS-CoV-2 infection. In all samples where SARS-CoV-2 RNA was detected by ddPCR, we performed qRT-PCR to detect subgenomic (sg)RNA, an assay suggestive of recent virus replication[15]. We confirmed the presence of replication-competent SARS-CoV-2 in extrapulmonary tissues by virus isolation in cell culture. Lastly, in six

individuals, we measured the diversity and anatomic distribution of intra-individual SARS-CoV-2 variants using high-throughput, single-genome amplification and sequencing (HT-SGS).

We categorized autopsy cases of SARS-CoV-2 infection as "early" (n=17), "mid" (n=13), or "late" (n=14) by illness day (D) at the time of death, being ≤D14, D15-D30, or ≥D31, respectively. We defined persistence as presence of SARS-CoV-2 RNA among late cases. Due to the extensive tissue collection, we analyzed and described the results in terms of grouped tissue categories as the following: respiratory tract; cardiovascular; lymphoid; gastrointestinal; renal and endocrine; reproductive; muscle, skin, adipose, & peripheral nerves; and brain.

Autopsy cohort overview

Between April 26, 2020 and March 2, 2021, we performed autopsies on 44 PCR-confirmed cases (Extended Data Fig. 1). SARS-CoV-2 seroconversion was detected in 38 of these cases (Supplementary Data 1); three early cases (P27, P36, P37) had not seroconverted and perimortem plasma was unavailable for the other three cases (P3, P4, P15). Extensive sampling of the brain was accomplished in 11 of the 44 cases (Fig. 1). The cohort was 29.5% female with a mean age of 59.2 years and was diverse across race and ethnicity (Extended Data Table 1). 95.5% of patients had at least one comorbidity, with hypertension (54.5%), obesity (52.3%), and chronic respiratory disease (34.1%) being most common. Patients presented to the hospital a mean of 9.4 days following symptom onset and were hospitalized a mean of 26.4 days. Overall, the mean interval from symptom onset to death was 35.2 days and the mean postmortem interval was 26.2 hours. 81.8% of patients required intubation with invasive mechanical ventilation, 22.7% received extracorporeal membrane oxygenation (ECMO) support, and 40.9% required renal replacement therapy. Vasopressors, systemic steroids, systemic anticoagulation, and

antibiotics were commonly administered (Extended Data Table 1). Individual patient-level demographic and clinical information can be found in Extended Data Table 2.

Widespread infection and persistence

SARS-CoV-2 RNA was detected in all 44 cases and across 79 of 85 anatomical locations and body fluids sampled (Extended Data Fig. 2, Supplementary Data 1). The highest burden of SARS-CoV-2 RNA (i.e., >100,000 N gene copies/ng RNA input) was detected in the respiratory tract of early cases (Figure 1), but we detected at least 100 N gene copies/ng RNA input from every tissue group besides reproductive tissues from multiple individuals among early cases. The mean SARS-CoV-2 N gene copies/ng RNA detected from tissues in each grouping among early cases are as follows: 9,210.10 across respiratory tissues; 38.75 across cardiovascular tissues; 30.01 across lymphoid tissues; 24.68 across gastrointestinal tissues; 12.76 across renal and endocrine tissues; 0.36 across reproductive tissues; 27.50 across muscle, peripheral nerve, adipose, and skin tissues; 57.40 across ocular tissues; and 32.93 across brain tissues (Extended Data Table 3).

With a few exceptions, the overall burden of SARS-CoV-2 RNA decreased by a log or more across tissue categories among mid cases, and further decreased among late cases. However, several mid and late cases had high levels (≥5 N gene copies/ng RNA input) detected among multiple tissues (Extended Data Fig. 2). Further, persistence of low-level SARS-CoV-2 RNA (0.0004 to <0.5 N gene copies/ng RNA input) was frequently detected across multiple tissue categories among all late cases, despite being undetectable in plasma (Extended Data Fig. 2, Supplementary Data 1). Notably, SARS-CoV-2 RNA was detected in the brains of all six late

158 cases and across most locations evaluated in the brain in five of these six, including P42 who
159 died at D230 (Fig. 1).
160 Overall, SARS-CoV-2 RNA was detected in respiratory tissue of 43/44 cases (97.7%);
161 cardiovascular tissue of 35/44 cases (79.5%); lymphoid tissue of 38/44 cases (86.4%);
162 gastrointestinal tissue of 32/44 (72.7%); renal and endocrine tissue of 28/44 cases (63.6%);
163 reproductive tissue in 17/40 cases (42.5%); muscle, skin, adipose, and peripheral nervous tissue
164 in 30/44 cases (68.2%); ocular tissue and humors of 22/28 cases (57.9%); and brain tissue in
165 10/11 cases (90.9%) (Extended Data Table 3).
166 We additionally detected SARS-CoV-2 sgRNA across all tissue categories,
167 predominately among early cases (14/17, 82.4%), as well as in plasma, pleural fluid, and vitreous
168 humor (Fig. 1, Extended Data Fig. 2, Supplementary Data 1). sgRNA was also detected in at
169 least one tissue of 61.5% of mid cases and 42.9% of late cases, including across three tissue
170 categories in a case at D99 (P20).
171 We isolated SARS-CoV-2 in cell culture from multiple pulmonary and extrapulmonary
172 tissues, including lung, bronchus, sinus turbinate, heart, mediastinal lymph node, small intestine,
173 and adrenal gland from early cases up to D7 (P19, P27, P32, P37; Supplementary Data 1).
174
175 **Intra-individual viral variant diversity**
176 We used HT-SGS to analyze SARS-CoV-2 spike gene variant sequences from a total of
177 46 tissues in six individuals. In five individuals from the early group, predominant spike
178 sequences were largely identical across tissues. In P27, P19, and P18, no non-synonymous virus
179 genetic diversity was detected in pulmonary and extrapulmonary sites despite a high depth of
180 single-molecule sampling (Extended Data Fig. 3). Thus, virus populations that were relatively

181 homogeneous had disseminated in these individuals without coding changes in spike. However,
182 we also noted important patterns of intra-individual virus diversity in several patients from the
183 early group. In P27, although all 4,525 inferred spike amino acid sequences were identical, two
184 virus haplotypes, each with a single synonymous substitution, were preferentially detected in
185 extrapulmonary sites including right and left ventricles and mediastinal LN. In P38, we observed
186 clear virus genetic differences between the lung lobes and the brain, with a D80F residue found
187 in 31/31 pulmonary but 0/490 brain sequences and a G1219V residue that was restricted to brain
188 minor variants. A similar distinction was observed between sequences from dura mater and other
189 sites in P36, albeit at very low sampling depth (n = 2 sequences) from dura mater. Overall, these
190 findings suggested no need for alterations in receptor utilization to permit extrapulmonary
191 dissemination of SARS-CoV-2, while also revealing genetic compartmentalization between
192 viruses in the lung lobes and those in extrapulmonary sites, including the brain.
193
194 **ISH reveals SARS-CoV-2 cellular tropism**
195 We validated our ddPCR results across all tissue categories via ISH for SARS-CoV-2
196 spike RNA across selected early, mid, and late cases (Supplementary Data 3). Overall, we
197 detected SARS-CoV-2 RNA via ISH in 36 distinct cell types across all sampled organs
198 (Extended Data Table 4, Supplementary Data 3). Spike RNA was detected throughout the
199 respiratory tract in early cases, as well as within the sinus turbinate, trachea, lungs, from late
200 cases (i.e., P33, P20, P42).
201 The heart contained spike RNA within myocytes, endothelium, and smooth muscle of
202 vessels of both early (P18, P19) and late (P3 & P42) cases. The pericardium demonstrated a
203 positive signal for spike RNA within fibroblasts of the stroma. Intimal cells of the aorta were

additionally found to contain spike RNA. Mononuclear leukocytes within the lymph node, spleen, and appendix of an early case (P19) contained spike RNA, as did colonic epithelium (Fig 2).

Epithelial cells along the intestinal tract in early cases (P16, P18, P19) contained viral RNA, as well as stratified squamous epithelium of the esophagus. Mononuclear leukocytes were again visualized with SARS-CoV-2 RNA in lymphoid aggregates and the interstitium of the small and large intestine, with infected cells still present in the colon of late cases (P33, P42). Kupffer cells, hepatocytes, and bile duct epithelium within the liver were additionally found to contain spike RNA.

Within the kidney, spike RNA could be visualized within parietal epithelium of Bowman's capsule, collecting duct cells, distal tubule cells, and glomerular endothelium. The adrenal glands contained spike RNA within endocrine cells. Endocrine follicular cells of the thyroid and glandular cells of the pancreas were also positive for spike RNA (Fig. 2). Among reproductive organs, spike RNA was visualized within Leydig and Sertoli cells of the testis, germ cells within the testicular tubules, endometrial gland epithelium, endometrial stromal cells, uterine smooth muscle cells, and stromal cells of the post-menopause ovary (Fig. 2).

Myocytes within skeletal muscle contained spike RNA in both early (P18) and late (P20) cases. In addition to the organ-specific cell type infection of SARS-CoV-2, endothelium, muscularis of atrial vessels, and Schwann cells were identified as infected throughout the body, and were similarly positive across early and late cases.

Spike RNA was found in neurons, glia and ependyma, as well as endothelium of vessels across all lobes of the brain of early, mid, and late cases. Within the cerebellum specifically,

neurons, Purkinje cells, and endothelium of vasculature also contained spike protein via IHC (Fig. 3).

COVID-19 histological findings

The histopathology findings from our cohort were similar to those reported in other case series (Extended Data Fig. 4). All but five cases were considered to have died from COVID-19 (Extended Data Table 5), and, of these, 37 (94.5%) had either acute pneumonia or diffuse alveolar damage at the time of death (Supplementary Data 2). Phases of diffuse alveolar damage showed clear temporal associations, with the exudative phase seen mainly within the first three weeks of infection and the fibrosing phase not seen until after a month of infection (Extended Data Fig. 5). Pulmonary thromboembolic complications, which were also likely related to SARS-CoV-2 infection, with or without infarction, were noted in 10 (23%) cases. Another finding likely related to SARS-CoV-2 infection included myocardial infiltrates in four cases, including one case of significant myocarditis[16] (P3). Some of the cases of microscopic ischemia appeared to be associated with fibrin-platelet microthrombi, and may therefore be related to COVID-19 thrombotic complications. Within the lymph nodes and spleen, we observed lymphodepletion and both follicular and paracortical hyperplasia.

Outside the lungs, histological changes were mainly related to complications of therapy or preexisting co-morbidities: mainly obesity, diabetes, and hypertension. Five cases had old ischemic myocardial scars and three had coronary artery bypass grafts in place. Given the prevalence of diabetes and obesity in our cohort, it was not surprising to find diabetic nephropathy (10 cases, 23%) or steatohepatitis (5 cases, 12%). One case was known to have chronic hepatitis C with cirrhosis, but the other cases of advanced hepatic fibrosis were likely

related to fatty liver disease, even if diagnostic features of steatohepatitis were not present. Hepatic necrosis (13 cases, 30%) and changes consistent with acute kidney injury (17 cases, 39%) were likely related to hypoxic-ischemic injury in these very ill patients.

In the examination of the 11 brains, we found few histopathologic changes, despite the evidence of substantial viral burden. Vascular congestion was an unusual finding that had an unclear etiology and could be related to the hemodynamic changes incurred with infection. Global hypoxic/ischemic change was seen in two cases, one of which was a juvenile (P36) with a seizure disorder who was found to be SARS-CoV-2 positive on hospital admission, but who likely died of seizure complications unrelated to viral infection.

Discussion

Here we provide the most comprehensive analysis to date of SARS-CoV-2 cellular tropism, quantification, and persistence across the body and brain, in a diverse autopsy cohort collected throughout the first year of the pandemic in the United States. Our focus on short post-mortem intervals, comprehensive approach to tissue collection, and preservation techniques – RNA*later* and flash freezing of fresh tissue – allowed us to detect and quantify viral levels with high sensitivity by ddPCR and ISH, as well as culture virus, which are notable differences compared to other studies.

We show SARS-CoV-2 disseminates across the human body and brain early in infection at high levels, and provide evidence of virus replication at multiple extrapulmonary sites during the first week following symptom onset. We detected sgRNA in at least one tissue in over half of cases (14/27) beyond D14, suggesting that prolonged viral replication may occur in extra-pulmonary tissues as late as D99. While others have questioned if extrapulmonary viral presence

is due to either residual blood within the tissue[8,17] or cross-contamination from the lungs during tissue procurement[8], our data rule out both theories. Only 12 cases had detectable SARS-CoV-2 RNA in a perimortem plasma sample, and of these only two early cases also had SARS-CoV-2 sgRNA in the plasma, which occurred at Ct levels higher than nearly all of their tissues with sgRNA. Therefore, residual blood contamination cannot account for RNA levels within tissues. Furthermore, blood contamination would not account for the SARS-CoV-2 sgRNA or virus isolated from tissues. Contamination of additional tissues during procurement, is likewise ruled out by ISH demonstrating widespread SARS-CoV-2 cellular tropism across the sampled organs, by IHC detecting viral protein in the brain, and by several cases of virus genetic compartmentalization in which spike variant sequences that were abundant in extrapulmonary tissues were rare or undetected in lung samples.

Using both ddPCR and sgRNA analysis to inform our selection of tissue for virus isolation and ISH staining allow us to describe a number of novel findings. Others[6,8-12,17] have previously reported SARS-CoV-2 RNA within the heart, lymph node, small intestine, and adrenal gland. We demonstrate conclusively that SARS-CoV-2 is capable of infecting and replicating within these tissues. Current literature has also reported absent or controversial expression of ACE2 and/or TMPRSS2 in several extrapulmonary tissues, such as the colon, lymphoid tissues, and ocular tissues, calling into question if these tissues can become infected by SARS-CoV-2[1-3]. However, we observed high levels of SARS-CoV-2 RNA and evidence of replication within these organs, as well as SARS-CoV-2 RNA via ISH in colonic mucosal epithelium and mononuclear leukocytes within the spleen, thoracic cavity lymph nodes, and GI lymphoid aggregates. We believe these ISH positive cells represent either infection or

phagocytized virus in resident macrophages. Further, we isolated virus from a mediastinal lymph node and ocular tissue from two early cases (P19, P32).

Our use of a single-copy sequencing approach for the SARS-CoV-2 spike allowed us to demonstrate homogeneous virus populations in many tissues, while also revealing informative virus variants in others. Low intra-individual diversity of SARS-CoV-2 sequences has been observed frequently in previous studies[18-20], and likely relates to the intrinsic mutation rate of the virus as well as lack of early immune pressure to drive virus evolution in new infections. It is important to note that our HT-SGS approach has both a high accuracy and a high sensitivity for minor variants within each sample, making findings of low virus diversity highly reliable[21]. The virus genetic compartmentalization that we observed between pulmonary and extrapulmonary sites in several individuals supports independent replication of the virus at these sites, rather than spillover from one site to another. Importantly, lack of compartmentalization between these sites in other individuals does not rule out independent virus replication, as independently replicating populations may share identical sequences if overall diversity is very low. It was also interesting to note several cases where brain-derived virus spike sequences showed non-synonymous differences relative to sequences from other tissues. These differences may indicate differential selective pressure on spike by antiviral antibodies in brain versus other sites, though further studies will be needed to confirm this speculation.

Our results collectively show while that the highest burden of SARS-CoV-2 is in the airways and lung, the virus can disseminate early during infection and infect cells throughout the entire body, including widely throughout the brain. While others have posited this viral dissemination occurs through cell trafficking[11] due to a reported failure to culture virus from blood[3,22], our data support an early viremic phase, which seeds the virus throughout the body

following pulmonary infection. Recent work by Jacobs et al.[22] in which SARS-CoV-2 virions were pelleted and imaged from COVID-19 patient plasma, supports this mechanism of viral dissemination. Although our cohort is primarily made up of severe cases of COVID-19, two early cases had mild respiratory symptoms (P28; fatal pulmonary embolism occurred at home) or no symptoms (P36; diagnosed upon hospitalization for ultimately fatal complications of a comorbidity), yet still had SARS-CoV-2 RNA widely detected across the body, including brain, with detection of sgRNA in multiple compartments. Our findings, therefore, suggest viremia leading to body-wide dissemination, including across the blood-brain barrier, and viral replication can occur early in COVID-19, even in asymptomatic or mild cases. Further, P36 was a juvenile with no evidence of multisystem inflammatory syndrome in children, suggesting infected children without severe COVID-19 can also experience systemic infection with SARS-CoV-2.

Finally, a major contribution of our work is a greater understanding of the duration and locations at which SARS-CoV-2 can persist. While the respiratory tract was the most common location in which SARS-CoV-2 RNA tends to linger, ≥50% of late cases also had persistence in the myocardium, thoracic cavity lymph nodes, tongue, peripheral nerves, ocular tissue, and in all sampled areas of the brain, except the dura mater. Interestingly, despite having much lower levels of SARS-CoV-2 in early cases compared to respiratory tissues, we found similar levels between pulmonary and the extrapulmonary tissue categories in late cases. This less efficient viral clearance in extrapulmonary tissues is perhaps related to a less robust innate and adaptive immune response outside the respiratory tract.

We detected sgRNA in tissue of over 60% of the cohort. While less definitive than viral culture[23,24], multiple studies have shown that sgRNA levels correlate with acute infection and can

be detected in respiratory samples of immunocompromised patients experiencing prolonged infection[24]. These data coupled with ISH suggest that SARS-CoV-2 can replicate within tissue for over 3 months after infection in some individuals, with RNA failing to clear from multiple compartments for up to D230. This persistence of viral RNA and sgRNA may represent infection with defective virus, which has been described in persistent infection with measles virus – another single-strand enveloped RNA virus—in cases of subacute sclerosing panencephalitis[25].

The mechanisms contributing to PASC are still being investigated; however, ongoing systemic and local inflammatory responses have been proposed to play a role[5]. Our data provide evidence for delayed viral clearance, but do not support significant inflammation outside of the respiratory tract even among patients who died months after symptom onset. Understanding the mechanisms by which SARS-CoV-2 persists and the cellular and subcellular host responses to viral persistence promises to improve the understanding and clinical management of PASC.

Main References:

1. Bourgonje, A. R. *et al*. Angiotensin-converting enzyme 2 (ACE2), SARS-CoV-2 and the pathophysiology of coronavirus disease 2019 (COVID-19). *J Pathol*. **251**(3), 228-248 (2020). https://doi.org/10.1002/path.5471.
2. Salamanna, F., Maglio, M., Landini. M. P., & Fini, M. Body Localization of ACE-2: On the Trail of the Keyhole of SARS-CoV-2. *Front Med (Lausanne)*. **7**, 594495 (2021). https://doi.org/10.3389/fmed.2020.594495.
3. Sridhar, S., & Nicholls, J. Pathophysiology of infection with SARS-CoV-2-What is known and what remains a mystery. *Respirology*. **26**(7), 652-665 (2021). https://doi.org/10.1111/resp.14091.
4. Al-Aly, Z., Xie, Y., & Bowe, B. High-dimensional characterization of post-acute sequelae of COVID-19. *Nature*. **594**(7862), 259-264 (2021). https://doi.org/10.1038/s41586-021-03553-9.
5. Crook, H., Raza, S., Nowell, J., Young, M., & Edison, P. Long covid-mechanisms, risk factors, and management. *BMJ*. **374**, n1648 (2021). https://doi.org/10.1136/bmj.n1648.
6. Puelles, V. G., *et al*. Multiorgan and Renal Tropism of SARS-CoV-2. *N Engl J Med*. **383**(6), 590-592 (2020). https://doi.org/10.1056/NEJMc2011400.
7. Martines, R. B., *et al*. Pathology and Pathogenesis of SARS-CoV-2 Associated with Fatal Coronavirus Disease, United States. *Emerg Infect Dis*. **26**(9), 2005-2015 (2020). https://doi.org/10.3201/eid2609.202095.
8. Bhatnagar, J., *et al*. Evidence of Severe Acute Respiratory Syndrome Coronavirus 2 Replication and Tropism in the Lungs, Airways, and Vascular Endothelium of Patients

With Fatal Coronavirus Disease 2019: An Autopsy Case Series. *J Infect Dis*. **223**(5), 752-764 (2021). https://doi.org/10.1093/infdis/jiab039.

9. Dorward, D. A., *et al*. Tissue-Specific Immunopathology in Fatal COVID-19. *Am J Respir Crit Care Med*. **203**(2),192-201 (2021). https://doi.org/10.1164/rccm.202008-3265OC.
10. Schurink, B., *et al*. Viral presence and immunopathology in patients with lethal COVID-19: a prospective autopsy cohort study. *Lancet Microbe*. **1**(7), e290-e299 (2020). https://doi.org/10.1016/S2666-5247(20)30144-0.
11. Yao, X.H., *et al*. A cohort autopsy study defines COVID-19 systemic pathogenesis. *Cell Res*. **31**(8), 836-846 (2021). https://doi.org/10.1038/s41422-021-00523-8.
12. Remmelink, M., et al. Unspecific post-mortem findings despite multiorgan viral spread in COVID-19 patients. *Crit Care*. **24**(10), 495 (2020). https://doi.org/10.1186/s13054-020-03218-5.
13. Mukerji, S. S., & Solomon, I. H. What can we learn from brain autopsies in COVID-19? *Neurosci Lett*. **742**, 135528 (2021). https://doi.org/10.1016/j.neulet.2020.135528.
14. Matschke, J., et al. Neuropathology of patients with COVID-19 in Germany: a post-mortem case series. *Lancet Neurol*. **19**(11), 919-929 (2020). https://doi.org/10.1016/S1474-4422(20)30308-2.
15. Speranza, E., et al. Single-cell RNA sequencing reveals SARS-CoV-2 infection dynamics in lungs of African green monkeys. *Sci Transl Med*. **13**(578), eabe8146 (2021). https://doi.org/10.1126/scitranslmed.abe8146
16. Vannella, K. M., et al. Evidence of SARS-CoV-2-specific T-cell-mediated myocarditis in a MIS-A case. *Front Imunol*. Accepted (manuscript ID: 779026).

17. Desai, N., et al. Temporal and spatial heterogeneity of host response to SARS-CoV-2 pulmonary infection. *Nat Commun*. **11**(1), 6319 (2020). https://doi.org/10.1038/s41467-020-20139-7.

18. Tonkin-Hill, G., et al. Patterns of within-host genetic diversity in SARS-CoV-2. *Elife*. **10**, e66857 (2021). https://doi.org/10.7554/eLife.66857.

19. Lythgoe, K. A., et al. SARS-CoV-2 within-host diversity and transmission. *Science*. **372**(6539), eabg0821 (2021). https://doi.org/10.1126/science.abg0821.

20. Valesano, A. L., et al. Temporal dynamics of SARS-CoV-2 mutation accumulation within and across infected hosts. *PLoS Pathog*. **17**(4), e1009499 (2021). https://doi.org/10.1371/journal.ppat.1009499.

21. Ko, S. H., et al. High-throughput, single-copy sequencing reveals SARS-CoV-2 spike variants coincident with mounting humoral immunity during acute COVID-19. *PLoS Pathog*. 17(4), e1009431 (2021). https://doi.org/10.1371/journal.ppat.1009431.

22. Jacobs, J. L., *et al*. SARS-CoV-2 Viremia is Associated with COVID-19 Severity and Predicts Clinical Outcomes. *Clin Infect Dis*. **10**, ciab686 (2021). https://doi.org/10.1093/cid/ciab686.

23. Alexandersen, S., Chamings, A., & Bhatta, T. R. SARS-CoV-2 genomic and subgenomic RNAs in diagnostic samples are not an indicator of active replication. *Nat Commun*. **11**(1), 6059 (2020). https://doi.org/10.1038/s41467-020-19883-7.

24. Binnicker, M. J. Can Testing Predict SARS-CoV-2 Infectivity? The Potential for Certain Methods To Be Surrogates for Replication-Competent Virus. *J Clin Microbiol*. **59**(11), e0046921 (2021). https://doi.org/10.1128/JCM.00469-21.

25. Sidhu, M. S., et al. Defective measles virus in human subacute sclerosing panencephalitis brain. *Virology*. **202**(20), 631-641 (1994). https://doi.org/10.1006/viro.1994.1384.

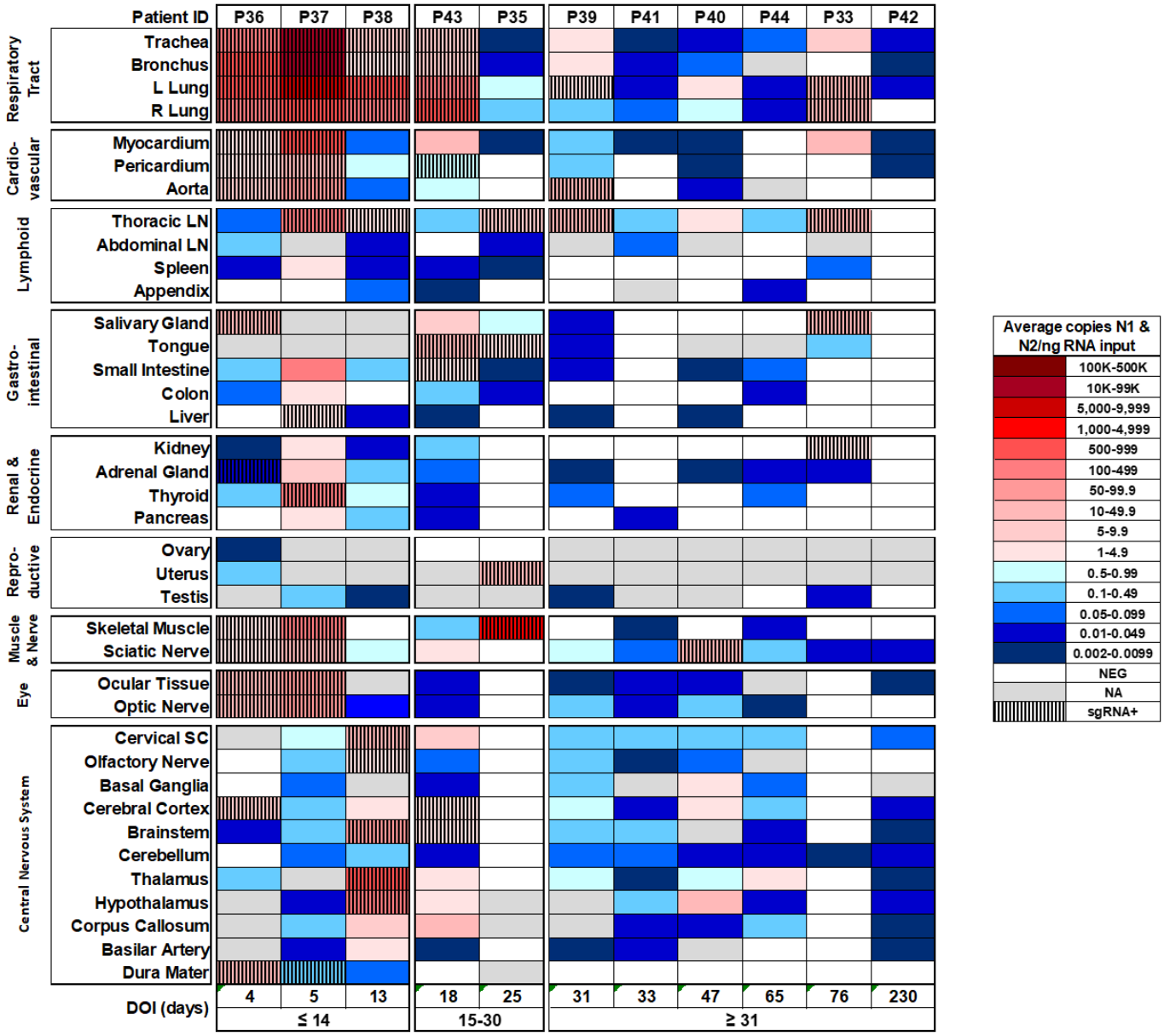

437

438 Fig. 1 **Distribution, quantification, and replication of SARS-Cov-2 across the human body**

439 **and brain.** The heat map depicts the highest mean quantification of SARS-CoV-2 RNA (N) via

440 ddPCR present within the tissues of eleven COVID-19 autopsy patients who underwent whole

441 body and brain sampling. Patients are aligned from shortest to longest duration of illness (DOI)

442 prior to death, listed at the bottom of the figure, and grouped into early (≤14 days), mid (15-30

443 days), and late (≥31 days) DOI. Tissues are grouped by tissue category beginning with the

444 respiratory tract at the top and central nervous system at the bottom. Viral RNA levels range
445 from 0.002 to 500,000 N gene copies per ng of RNA input, depicted as a gradient from dark blue
446 at the lowest level to dark red at the highest level. Tissues that were also positive for sgRNA via
447 real-time RT-PCR are shaded with black vertical bars. L/left, LN/lymph node, NA/not acquired,
448 R/right, SC/spinal cord.
449
450
451
452
453
454
455
456
457
458
459

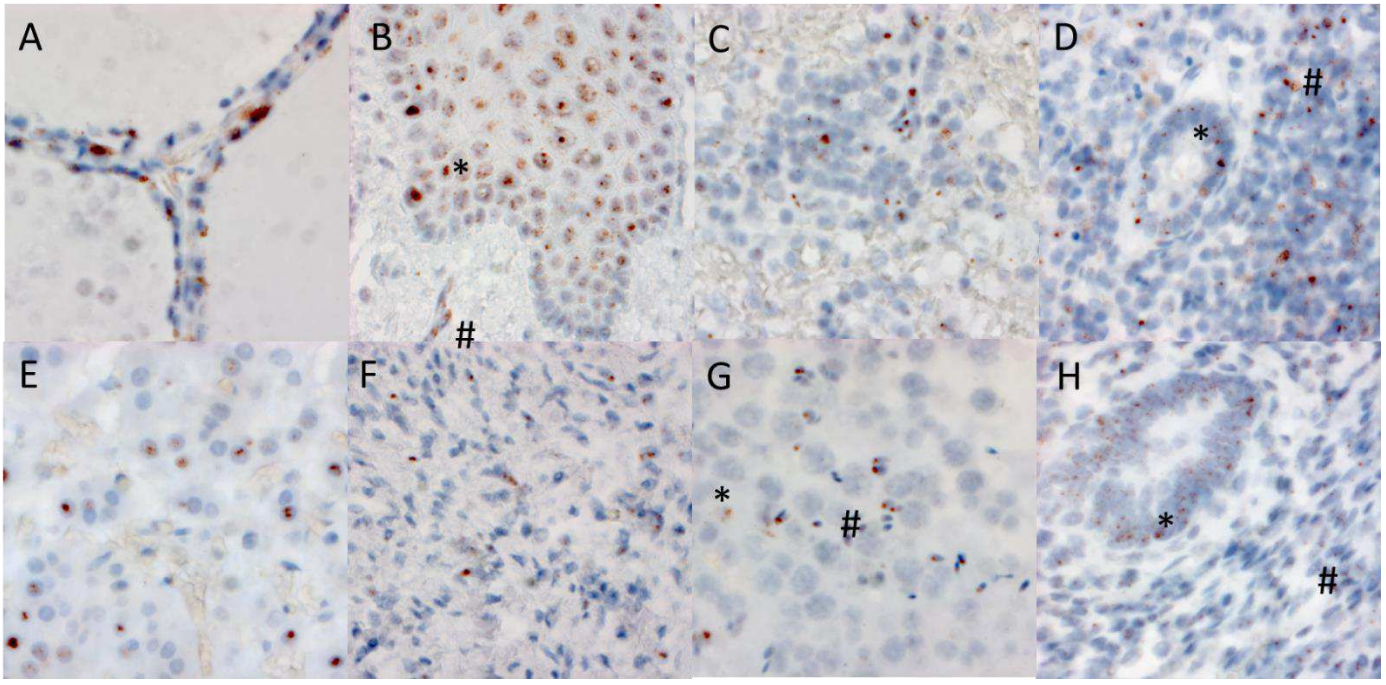

Fig. 2 **RNA *in situ* (RNAscope) detection of SARS-CoV-2 in extrapulmonary tissues**. SARS-CoV-2 virus is localized to the Golgi and endoplasmic, peri-nuclear in appearance, in the following organs and cell types (500 X magnifications): A) Thyroid, demonstrating presence of virus within follicular cells. B) Esophagus, demonstrating the presence of virus within the stratified squamous epithelium (*), as well as signal in capillaries within the stroma (#). C. Spleen, demonstrating the presence of mononuclear lymphoid cells within the white pulp. D) Appendix, demonstrating the presence of virus in both colonic epithelium (*) and mononuclear lymphoid cells in the stroma (#). E) Adrenal demonstrates virus within endocrine secretory cells of the adrenal gland. F) Ovary demonstrates the presence of virus in stromal cells of the ovary in a post-menopausal ovary. G) Testis demonstrates the presence of virus in both Sertoli cells (*) and maturing germ cells within the seminiferous tubules of the testis (#). H) Endometrium demonstrates the presence of virus within endometrial gland epithelium (*) and stromal cells (#), in a pre-menopausal endometrial sample.

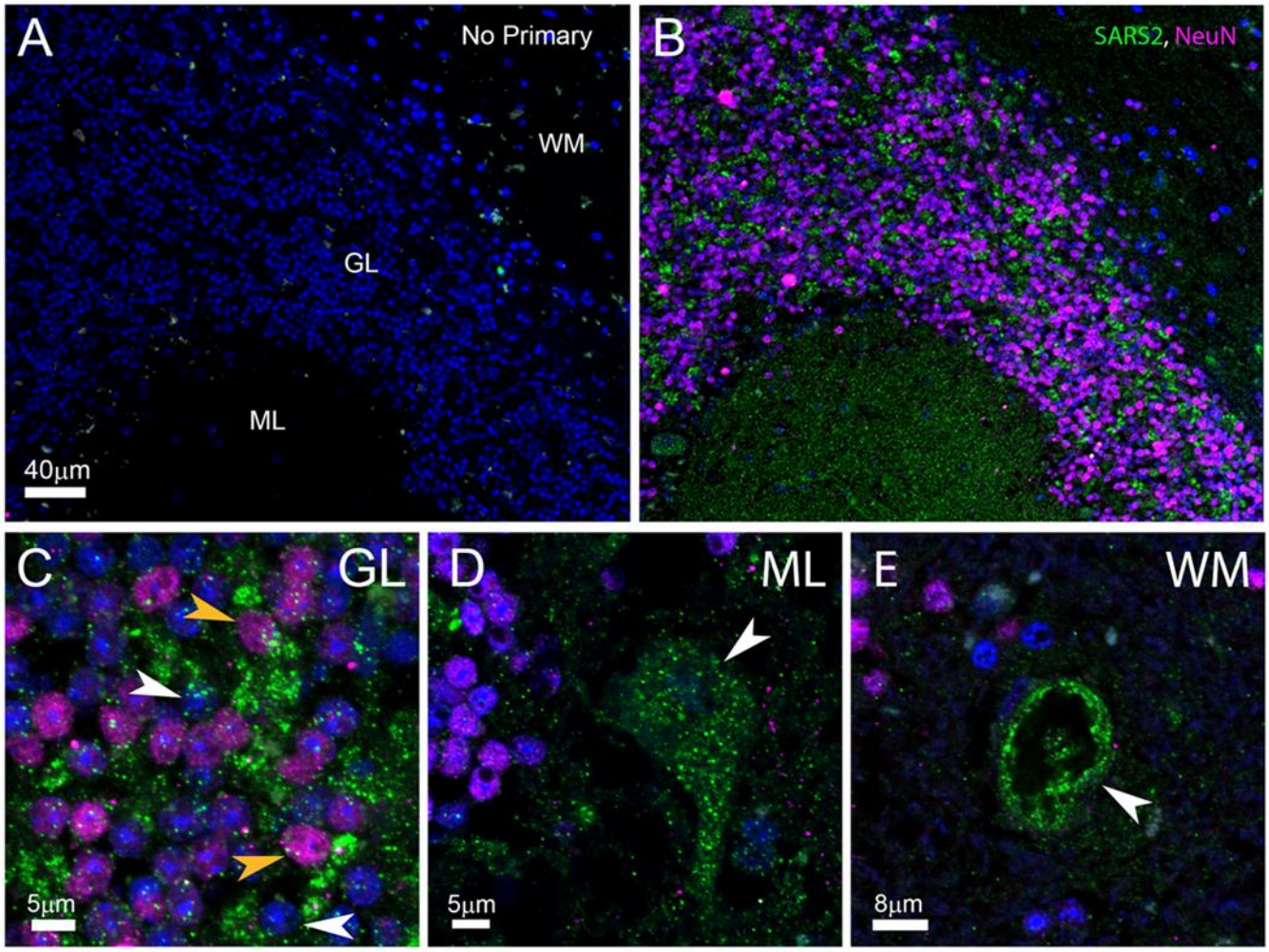

Fig. 3 **SARS-CoV-2 protein expression in human cerebellum**. Low magnification visualization of no-primary control (A) and primary-added adjacent (B) cerebellar sections labeled for SARS-CoV-2 (green) and NeuN (magenta) demonstrate viral-specific protein expression within the tissue. The locations of the molecular layer (ML), granular layer (GL), and white matter (WM) are indicated in (A) and also correspond to (B). Higher magnification images demonstrate cell type-specific infection (C-E). Both NeuN positive neurons (yellow arrows) and other unidentified cells (white arrows) are associated with viral protein in the GL (C). Purkinje cells adjacent to the ML are infected (D, white arrow). In rare instances, blood vessels adjacent

to the GL and WM were associated with viral protein (E, white arrow). The scale bars in A is also associated with B. All immunofluorescent images were obtained by confocal microscopy.

Methods:

Autopsies

Autopsies were performed and tissues were collected as previously described[26] in the National Cancer Institute's Laboratory of Pathology at the National Institutes of Health Clinical Center following consent of the legal next of kin.

Measurement of IgG and IgM antibodies against Nucleocapsid and Spike protein of SARS-CoV-2

Fluid-phase luciferase immunoprecipitation systems (LIPS) assays were used to study IgG and IgM antibody response to SARS-CoV-2. For IgG LIPS measurements, *Renilla* luciferase-nucleocapsid and *Gaussia* luciferase-spike protein extracts were employed with protein A/G beads (Protein A/G UltraLink Resin, Thermo Fisher Scientific) as the IgG capture reagent as previously described with microtiter filter plates[27]. For IgM measurements, anti-human IgM goat agarose beads (Sigma) were substituted as the capture reagent using both the microfilter plate and microtube format[28]. The IgM immunoprecipitation assays performed in 1.5 ml microfuge tube format containing 1 µl sera or plasma, *Renilla* luciferase-nucleocapsid (10 million light unit input per tube) or *Gaussia* luciferase-spike protein (40 million light input per tube) and buffer A (20 mM Tris, pH 7.5, 150 mM NaCl, 5 mM $MgCl_2$, 0.1% Triton X-100) to a total volume of 100 µl. After mixing, the tubes were incubated at room temp for 1 hour. Next 10 µl of the anti-human IgM agarose bead suspension was added to each tube for additional 60 minutes and tubes were placed on a rotating wheel at 4° C. The samples were then washed by brief centrifugation to collect the bead pellet at room temperature 3 times with 1.5 ml Buffer A and once with 1.5 ml of PBS. After the final wash, the beads were mixed with coelenterazine substrate (100 µl) and light

units measured in a tube luminometer. Known seronegative and seropositive samples for IgG and IgM antibodies against nucleocapsid and spike proteins were used for assigning seropositive cut-off values and for standardization.

SARS-CoV-2 RNA quantification of tissues and body fluids

Total RNA was extracted from RNAlater (Invitrogen)-preserved tissues and body fluids collected at autopsy using the RNeasy Mini, RNeasy Fibrous Tissue Mini, RNeasy Lipid Tissue Mini Kit, and QIAamp Viral RNA Mini Kits (Qiagen) according to the manufacturer's protocols. Upstream tissue processing and subsequent RNA quantification have been previously described[26]. The QX200 AutoDG Droplet Digital PCR System (Bio-Rad) was used to detect and quantify SARS-CoV-2 RNA in technical replicates of 5.5 uL RNA for fluids and up to 550 ng RNA for tissues as previously described[26]. Results were then normalized to copies of N1, N2, and RP per mL of sample input for fluids and per ng of RNA concentration input for tissues. For samples to be considered positive for SARS-CoV-2 N1 or N2 genes, they needed to mean the manufacturer's limit of detection of ≥0.1 copies/µL and ≥2 positive droplets per well. Over 60 control autopsy tissues from uninfected patients, representing all organs collected for COVID-19 autopsy cases, were used to validate the manufacturer's EUA published LOD for nasopharyngeal swabs for tissues (Extended Data Table 8). ddPCR data for P3[16] as well as a portion of tissues from the oral cavity[26] have been previously reported.

sgRNA analysis of ddPCR positive tissues

Tissues that tested positive for one or both SARS-CoV-2 N gene targets via ddPCR had RNA submitted for sgRNA analysis. Briefly, five µl RNA was used in a one-step real-time RT-PCR

assay to sgRNA (forward primer 5'- CGATCTCTTGTAGATCTGTTCTC-3'; reverse primer 5'-ATATTGCAGCAGTACGCACACA-3'; probe 5'-FAM-ACACTAGCCATCCTTACTGCGCTTCG-ZEN-IBHQ-3')[29] using the Rotor-Gene probe kit (Qiagen) according to instructions of the manufacturer. In each run, standard dilutions of counted RNA standards were run in parallel to calculate copy numbers in the samples. The limit of detection for this assay was determined to be <40 Cq (Supplemental Data 1) using 40 control autopsy tissues from uninfected patients, representing all organs collected for COVID-19 autopsy cases.

Viral isolation from select postmortem tissues

Select tissues with high viral RNA levels via ddPCR and sgRNA PCR measuring at or below a 30 Cq underwent virus isolation to prove the presence of infectious virus. Virus isolation was performed on tissues by homogenizing the tissue in 1ml DMEM and inoculating Vero E6 cells in a 24-well plate with 250 µl of cleared homogenate and a 1:10 dilution thereof. Plates were centrifuged for 30 minutes at 1000 rpm and incubated for 30 minutes at 37°C and 5% CO2. The inoculum was then removed and replaced with 500 µl DMEM containing 2% FBS, 50 U/ml penicillin and 50 µg/ml streptomycin. Six days after inoculation, cytopathic effect (CPE) was scored. A blind passage of samples where no CPE was present, was performed according to the same method. Supernatants from plates with CPE present were analyzed via PCR for SARS-CoV-2 to rule out other causes of CPE.

Virus Sequencing Methods

575 Patients with duration of illness ≤7 d (P27, P19) and 8-14 d (P18) with multiple body site
576 tissues containing sgRNA levels ≤31 Cq value were selected for high throughput, single-genome
577 amplification and sequencing (HT-SGS) as previously described[21]. Presence of variants of
578 SARS-CoV-2 were analyzed within and between tissues.
579
580 **SARS-CoV-2 RNA *in situ* hybridization**
581 Chromogenic *in situ* detection was performed using the manual RNAScope 2.5 HD assay (Cat#
582 322310, Advanced Cell Diagnostics, Hayward, CA) with a modified pretreatment protocol.
583 Briefly, formalin-fixed and paraffin-embedded (FFPE) tissue sections were cut at 7 μm, air dried
584 overnight, and baked for 2 hrs at 60ºC. The FFPE tissue sections were deparaffinized,
585 dehydrated, and then treated with pretreat 1 for 10 min at room temperature. The slides were
586 boiled with pretreatment reagent for 15 min, digested with protease at 40ºC for 10 min, then
587 hybridized for 2 hours at 40ºC with probe-*V-nCov2019-S* (Cat# 848561, Advanced Cell
588 Diagnostics). In addition, probe-Hs-*PPIB* (Cat# 313901, Advanced Cell Diagnostics) and probe-
589 *dapB* (Cat# 310043, Advanced Cell Diagnostics) were used as a positive and negative control,
590 respectively. Subsequent amplification was done according to the original protocol. Detection of
591 specific probe binding sites were visualized with RNAScope 2.5 HD Reagent kit-brown
592 chromogenic labels (Advanced Cell Diagnostics). The slides were counterstained with
593 hematoxylin and cover-slipped.
594
595 **SARS-CoV-2 immunohistochemistry**
596 FFPE cerebellar sections were deparaffinized, rehydrated and subject to 0.01M Citrate buffer
597 antigen retrieval for 20min at 120°C. Slides were incubated in 0.1% TritonX100 in PBS for

30min, washed extensively with PBS and fresh True Black Plus® solution (1:40, Cat#23014, Biotium) applied for 7min. Following PBS wash, blocking serum (5% normal donkey serum/0.3M glycine) was applied for 30min. Primary antibodies against SARS-CoV-2 NP1 (1:250, custom made) and NeuN (1:200, Cat#MAB377, Chemicon) were diluted in blocking serum and applied to slides overnight at 4°C. Species-specific secondary conjugates (1:500, Cat#A32790 and #A32744, ThermoFisher) were applied for 1hr at RT. Hoescht 33342 applied for 10min (1:2000, Cat#H3570, ThermoFisher) labeled nuclei. Slides were cover-slipped with Prolong Gold (Cat#P36930, ThermoFisher).

Data Availability

The datasets that support the findings of this study are available in Supplementary Data 1, 2 and 3. Sequence data described in this manuscript have been deposited (database accession numbers XXXX). The bioinformatic pipeline for HT-SGS data analysis has been deposited (https://github.com/niaid/UMI-pacbio-pipeline). ISH images from our cohort as well as positive and negative controls are available in Supplementary Data 3, which is available at https://halo.cancer.gov, Authentication method: NIH, username: halocancernci@gmail.com, password: covid19N!H.

Methods References:

26. Huang, N., et al. SARS-CoV-2 infection of the oral cavity and saliva. *Nat Med*. **27**, 892–903 (2021). https://doi.org/10.1038/s41591-021-01296-8.
27. Burbelo, P. D., et al. Sensitivity in Detection of Antibodies to Nucleocapsid and Spike Proteins of Severe Acute Respiratory Syndrome Coronavirus 2 in Patients With

Coronavirus Disease 2019. *J Infect Dis*. **222**(2), 206-213 (2020). https://doi.org/10.1093/infdis/jiaa273.

28. Burbelo, P. D., Goldman, R., & Mattson, T. L. A simplified immunoprecipitation method for quantitatively measuring antibody responses in clinical sera samples by using mammalian-produced Renilla luciferase-antigen fusion proteins. *BMC Biotechnol*. **5**, 22 (2005). https://doi.org/10.1186/1472-6750-5-22.
29. Wölfel R., et al. Virological assessment of hospitalized patients with COVID-19. *Nature*. **581**(7809), 465-469 (2020). https://doi.org/10.1038/s41586-020-2196-x.

Acknowledgements:

This study was funded and supported by the Intramural Research Program of the National Institutes of Health, Clinical Center, National Institute of Dental and Craniofacial Research, and National Institute of Allergy and Infectious Diseases.

This research was made possible through the NIH Medical Research Scholars Program, a public-private partnership supported jointly by the NIH and contributions to the Foundation for the NIH from the Doris Duke Charitable Foundation, Genentech, the American Association for Dental Research, and the Colgate-Palmolive Company.

NIH COVID-19 Autopsy Consortium

Daniel S. Chertow[1,2], Kevin M. Vannella[1,2], Sydney R. Stein[1,2], Marcos J. Ramos-Benitez[1,2,4], Andrew P. Platt[1,2], James M. Dickey[1,2], Ashley L. Babyak[1,2], Luis J. Perez Valencia[1,2], Sabrina C. Ramelli[3], Shelly J. Curran[3], Mary E. Richert[3], David E. Kleiner[5], Stephen M. Hewitt[5], Martha Quezado[5], Willie J. Young[5], Sarah P. Young[5], Billel Gasmi[5], Michelly Sampaio De Melo[5],

Sabina Desar[5], Saber Tadros[5], Nadia Nasir[5], Xueting Jin[5], Sharika Rajan[5], Esra Dikoglu[5], Neval Ozkaya[5], Kris Ylaya[5], Joon-Yong Chung[5], Stefania Pittaluga[5], Grace Smith[5], Elizabeth R. Emanuel[6], Brian L. Kelsall[6], Justin A. Olivera[7], Megan Blawas[7], Robert A. Star[7], Alison Grazioli[8], Nicole Hays[9], Madeleine Purcell[9], Shreya Singireddy[9], Jocelyn Wu[9], Katherine Raja[9], Ryan Curto[9], Jean E. Chung[10], Amy J. Borth[10], Kimberly A. Bowers[10], Anne M. Weichold[10], Paula A. Minor[10], Mir Ahmad N. Moshref[10], Emily E. Kelly[10], Mohammad M. Sajadi[11,12], Kapil K. Saharia[11,12], Daniel L. Herr[13], Thomas M. Scalea[14], Douglas Tran[15], Ronson J. Madathil[15], Siamak Dahi[15], Kristopher B. Deatrick[15], Eric M. Krause[16], Joseph Rabin[17], Joseph A. Herrold[18], Ali Tabatabai[18], Eric S. Hochberg[18], Christopher R. Cornachione[18], Andrea R. Levine[18], Justin E. Richards[19], John Elder[20], Allen P. Burke[20], Michael A. Mazzeffi[21], Robert H. Christenson[22], Zackary A. Chancer[23], Mustafa Abdulmahdi[24], Sabrina Sopha[24], Tyler Goldberg[24], Shahabuddin Soherwardi[25], Yashvir Sangwan[26], Michael T. McCurdy[27,12], Kristen Sudano[27], Diane Blume[27], Bethany Radin[27], Madhat Arnouk[27], James W. Eagan Jr[28], Robert Palermo[29], Anthony D. Harris[30]

Affiliations:

1. Emerging Pathogens Section, Department of Critical Care Medicine, Clinical Center, National Institutes of Health, Bethesda, MD, USA
2. Laboratory of Immunoregulation, National Institute of Allergy and Infectious Diseases, Bethesda, MD, USA
3. Critical Care Medicine Department, Clinical Center, National Institutes of Health, Bethesda, MD, USA

4. Postdoctoral Research Associate Training Program, National Institute of General Medical Sciences, National Institutes of Health, Bethesda, MD, USA
5. Laboratory of Pathology, Center for Cancer Research, National Cancer Institute, National Institutes of Health, Bethesda, MD, USA
6. Mucosal Immunobiology Section, Laboratory of Molecular Immunology, National Institute of Allergy and Infectious Diseases, National Institutes of Health, Bethesda, MD, USA
7. Renal Diagnostics and Therapeutics Unit, Kidney Diseases Branch, National Institute of Diabetes and Digestive and Kidney Diseases, National Institutes of Health, Bethesda, MD, USA
8. Kidney Disease Section, Kidney Diseases Branch, National Institute of Diabetes and Digestive and Kidney Diseases, National Institutes of Health, Bethesda, MD, USA
9. University of Maryland School of Medicine, Baltimore, MD, USA
10. University of Maryland Medical Center, Baltimore, MD, USA
11. Institute of Human Virology, University of Maryland School of Medicine, Baltimore, MD, USA
12. Department of Medicine, Division of Pulmonary and Critical Care Medicine, University of Maryland School of Medicine, Baltimore, MD, USA
13. R Adams Cowley Shock Trauma Center, Department of Medicine and Program in Trauma, University of Maryland School of Medicine, Baltimore, MD, USA
14. Department of Shock Trauma Critical Care, University of Maryland School of Medicine, Baltimore, MD, USA

15. Department of Surgery, Division of Cardiac Surgery, University of Maryland School of Medicine, Baltimore, MD, USA
16. Department of Surgery, Division of Thoracic Surgery, University of Maryland School of Medicine, Baltimore, MD, USA
17. R Adams Cowley Shock Trauma Center, Department of Surgery and Program in Trauma, University of Maryland School of Medicine, Baltimore, MD, USA
18. Department of Medicine, Division of Infectious Disease, University of Maryland School of Medicine, Baltimore, MD, USA
19. Department of Anesthesiology, Division of Critical Care Medicine, University of Maryland School of Medicine, Baltimore, MD, USA
20. Department of Autopsy and Thoracic Pathology, University of Maryland School of Medicine, Baltimore, MD, USA
21. Department of Anesthesiology and Critical Care Medicine, George Washington School of Medicine and Health Sciences, Washington, DC USA
22. Department of Laboratory Science, University of Maryland School of Medicine, Baltimore, MD, USA
23. Department of Anesthesiology, University of Southern California Keck School of Medicine, Los Angeles, CA, USA
24. Critical Care Medicine, University of Maryland Baltimore Washington Medical Center, Glen Burnie, MD, USA
25. Hospitalist Department, TidalHealth Peninsula Regional, Salisbury, MD, USA
26. Department of Interventional Pulmonology, TidalHealth Peninsula Regional, Salisbury, MD, USA

27. Division of Critical Care Medicine, Department of Medicine, University of Maryland St. Joseph Medical Center, Towson, MD, USA
28. Department of Pathology, University of Maryland, St. Joseph Medical Center, Towson, MD, USA
29. Department of Pathology, Greater Baltimore Medical Center, Townson, MD, USA
30. Department of Epidemiology and Public Health, University of Maryland School of Medicine, Baltimore, MD, USA

Author Contributions

DSC, KMV, SRS, MJRB, ALB, LJPV, AG, DLH, SMH & DEK contributed to the study design and protocols for autopsy procurement. APP, JMD, MER, AG, NH, MP, SS, JW, KR, RC, JEC, AJB, KAB, AMW, PAM, MANM, EEK, MMS, KKS, DLH, TMS, DT, RJM, SD, KBD, EMK, JR, JAH, AT, ESH, CRC, ARL, JER, JE, APB, MAM, RHC, ZAC, MA, SS, TG, SS, YS, MTM, KS, DB, BR, MA, JWE Jr, RP, and ADH provided care for, recruited, collected samples from, and/or procured medical records for the patients in this study. DEK, SMH, MQ, WJY, SPY, BG, MSDM, SD, ST, NN, XJ, SR, ED, NO, KY, JYC, SP, and GS conducted the autopsies and/or histological and ISH analysis. SRS, MJRB, APP, JMD, ALB, LJPV, SCR, SJC, ERE, BLK, JAO, MB, and RAS assisted with procurement and preservation of autopsy specimens. SRS with assistance from SCR and JMD performed RNA extraction, ddPCR, and data analysis. MS, CKY, VJM, and EDW performed and analyzed data for sgRNA RT-PCR. CWW and KEP conducted IHC on cerebellum. PDB and JIC measured antibody responses to SARS-CoV-2 in perimortem plasma samples. SHK, FB, and EAB performed viral sequencing. SRS drafted the manuscript with critical input from DSC, KMV, SMH, DEK, SCR, APP, MJRB, EDW, VJM, AG, DLH,

KKS, MMS MTM, PDB, JIC, CWW, KEP, and SJC. All authors approved the submitted version of the manuscript.

Competing Interests:

The authors declare no competing or conflict of interest.

Additional Information:

Supplementary information is available for this paper.

Correspondence and requests for materials should be addressed to DSC.

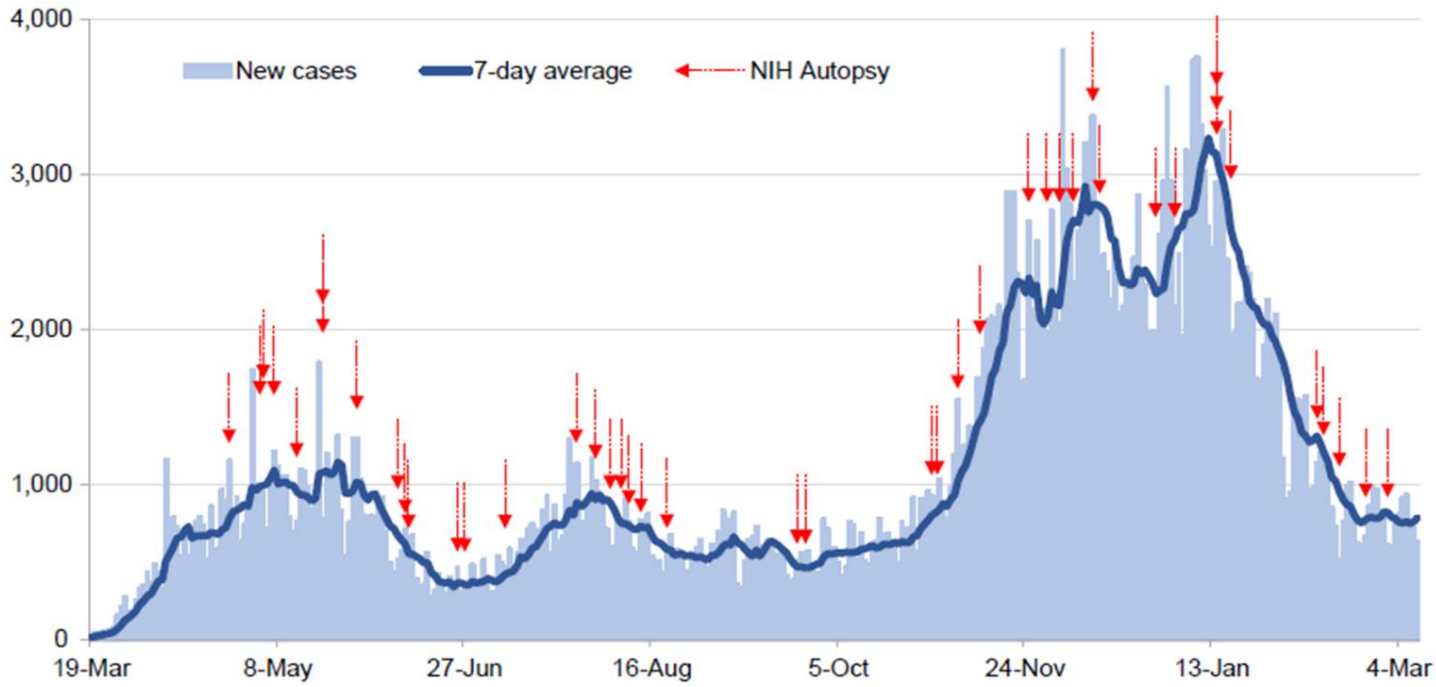

Extended Data Fig. 1 **Autopsy procurement relative to Maryland COVID-19 cases, March 19th, 2020 to March 9th, 2021**. Daily COVID-19 reported cases for Maryland (light blue bars) with 7-day average (dark blue line) with timing of autopsies (red arrows).

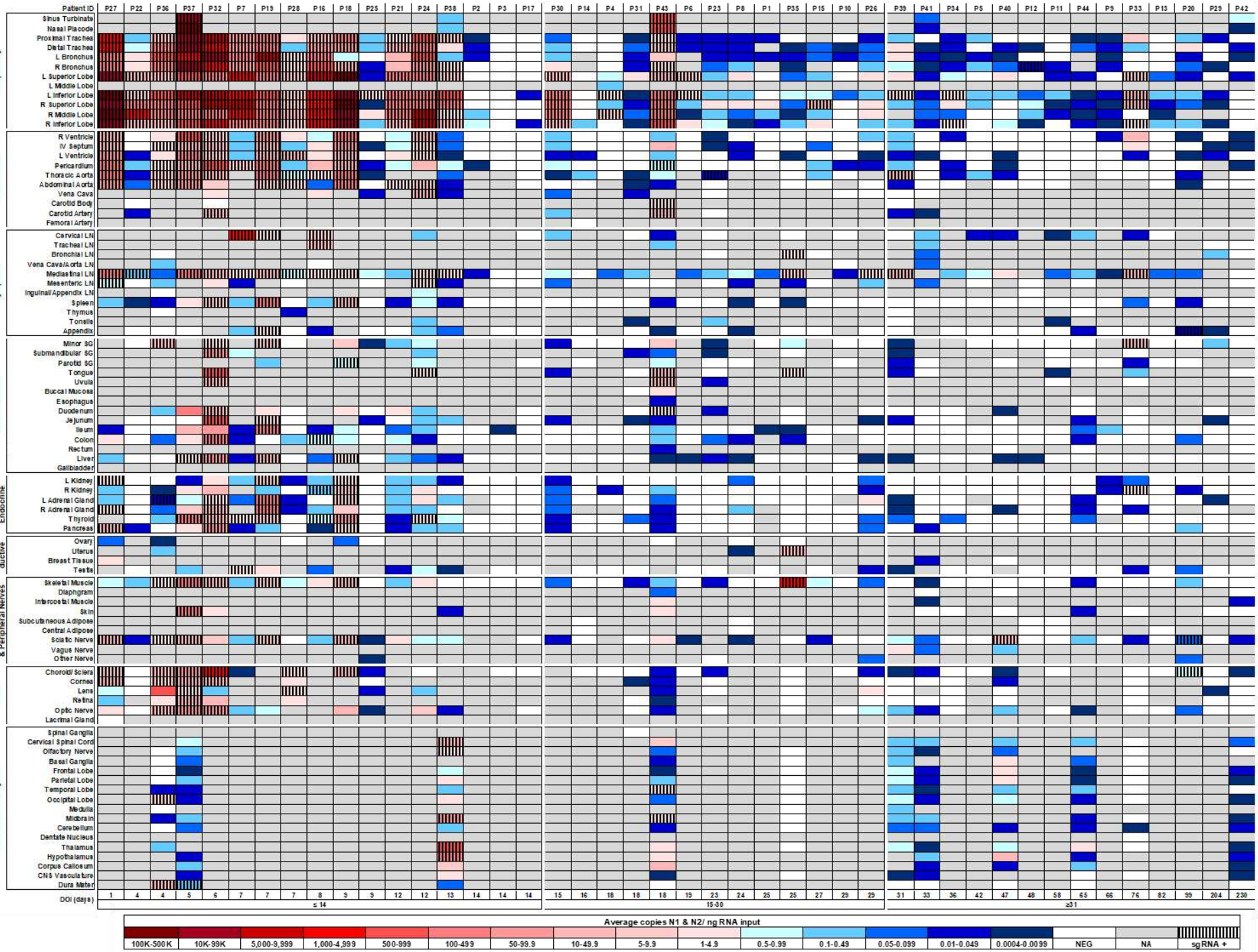
Patient ID
P27 P22 P36 P37 P32 P7 P19 P28 P16 P18 P25 P21 P24 P38 P2 P3 P17 P30 P14 P4 P31 P43 P6 P23 P8 P1 P35 P15 P10 P26 P39 P41 P34 P5 P40 P12 P11 P44 P9 P33 P13 P20 P29 P42
Respiratory
Sinus Turbinate
Nasal Placode
Proximal Trachea
Distal Trachea
L Bronchus
R Bronchus
L Superior Lobe
L Middle Lobe
L Inferior Lobe
R Superior Lobe
R Middle Lobe
R Inferior Lobe
Cardiovascular
R Ventricle
IV Septum
L Ventricle
Pericardium
Thoracic Aorta
Abdominal Aorta
Vena Cava
Carotid Body
Carotid Artery
Femoral Artery
Lymphoid
Cervical LN
Tracheal LN
Bronchial LN
Vena Cava/Aorta LN
Mediastinal LN
Mesenteric LN
Inguinal/Appendix LN
Spleen
Thymus
Tonsils
Appendix
Gastrointestinal
Minor SG
Submandibular SG
Parotid SG
Tongue
Uvula
Buccal Mucosa
Esophagus
Duodenum
Jejunum
Ileum
Colon
Rectum
Liver
Gallbladder
Renal & Endocrine
L Kidney
R Kidney
L Adrenal Gland
R Adrenal Gland
Thyroid
Pancreas
Repro-ductive
Ovary
Uterus
Breast Tissue
Testis
Muscle, Skin, Adipose & Peripheral Nerves
Skeletal Muscle
Diaphragm
Intercostal Muscle
Skin
Subcutaneous Adipose
Central Adipose
Sciatic Nerve
Vagus Nerve
Other Nerve
Ocular
Choroid/ Sclera
Cornea
Lens
Retina
Optic Nerve
Lacrimal Gland
Central Nervous System
Spinal Ganglia
Cervical Spinal Cord
Olfactory Nerve
Basal Ganglia
Frontal Lobe
Parietal Lobe
Temporal Lobe
Occipital Lobe
Medulla
Midbrain
Cerebellum
Dentate Nucleus
Thalamus
Hypothalamus
Corpus Callosum
CNS Vasculature
Dura Mater
DOI (days)
1 4 4 5 6 7 7 7 8 9 9 12 12 13 14 14 14 15 16 18 18 18 19 23 24 25 25 27 29 29 31 33 36 42 47 48 58 65 66 76 82 99 204 230
≤ 14
15-30
≥31
Average copies N1 & N2/ ng RNA input
100K-500K
10K-99K
5,000-9,999
1,000-4,999
500-999
100-499
50-99.9
10-49.9
5-9.9
1-4.9
0.5-0.99
0.1-0.49
0.05-0.099
0.01-0.049
0.0004-0.0099
NEG
NA
sgRNA +

Extended Data Fig. 2 **Distribution, quantification, and replication of SARS-CoV-2 across the body and brain over time.** The heat map depicts the highest average quantification of SARS-CoV-2 RNA (N) via ddPCR present within all sampled tissues of 44 autopsy cases. Patients are aligned from shortest to longest duration of illness (DOI) prior to death, listed at the bottom of the figure, and grouped into early (0-14 d), mid (15-30 d), and late (≥31 d) DOI. Tissues are grouped by body system beginning with the respiratory tract at the top and CNS at the bottom. Viral RNA levels range from 0.0004 to 500,000 copies per ng of RNA input, depicted as a gradient from dark blue at the lowest level to dark red at the highest level. Tissues that were also positive for sgRNA via real-time RT-PCR are shaded with black vertical bars.

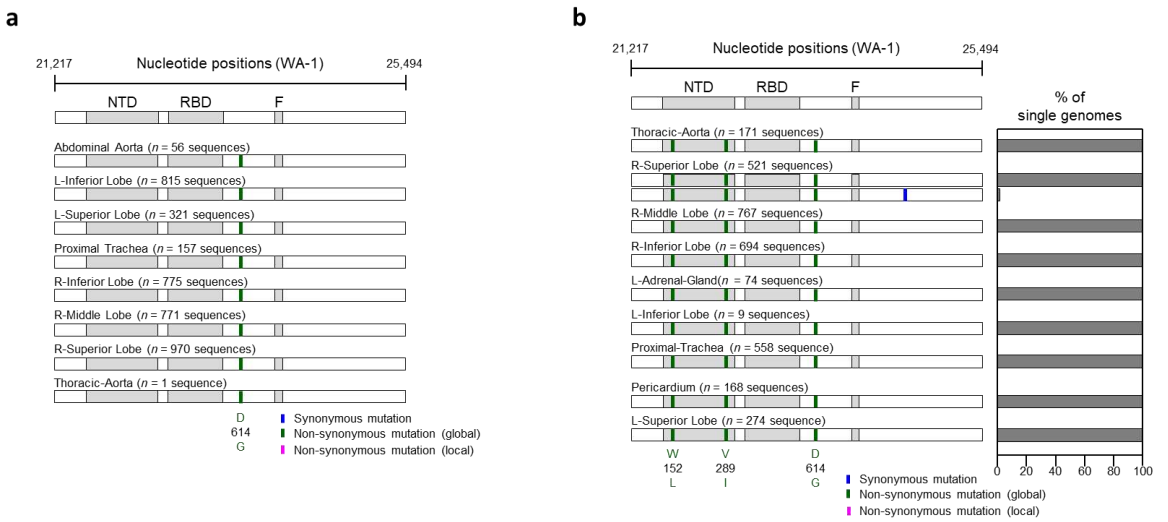
a
21,217
Nucleotide positions (WA-1)
25,494
NTD
RBD
F
Abdominal Aorta (n = 56 sequences)
L-Inferior Lobe (n = 815 sequences)
L-Superior Lobe (n = 321 sequences)
Proximal Trachea (n = 157 sequences)
R-Inferior Lobe (n = 775 sequences)
R-Middle Lobe (n = 771 sequences)
R-Superior Lobe (n = 970 sequences)
Thoracic-Aorta (n = 1 sequence)
D 614 G
Synonymous mutation
Non-synonymous mutation (global)
Non-synonymous mutation (local)
b
21,217
Nucleotide positions (WA-1)
25,494
NTD
RBD
F
% of single genomes
Thoracic-Aorta (n = 171 sequences)
R-Superior Lobe (n = 521 sequences)
R-Middle Lobe (n = 767 sequences)
R-Inferior Lobe (n = 694 sequences)
L-Adrenal-Gland(n = 74 sequences)
L-Inferior Lobe (n = 9 sequences)
Proximal-Trachea (n = 558 sequence)
Pericardium (n = 168 sequences)
L-Superior Lobe (n = 274 sequence)
W 152 L
V 289 I
D 614 G
0 20 40 60 80 100
Synonymous mutation
Non-synonymous mutation (global)
Non-synonymous mutation (local)
c
21,217
Nucleotide positions (WA-1)
25,494
NTD
RBD
F
% of single genomes
Abdominal-Aorta (n = 14 sequences)
L-Inferior Lobe (n = 521 sequences)
L-Superior Lobe (n = 282 sequences)
L-Ventricle (n = 484 sequences)
Mediastinal-LN (n = 840 sequences)
Proximal-Trachea (n = 204 sequences)
R-Inferior Lobe (n = 908 sequences)
R-Middle Lobe (n = 246 sequences)
R-Superior Lobe (n = 868 sequence)
R-Ventricle (n = 158 sequences)
D 614 G
0 20 40 60 80 100
Synonymous mutation
Non-synonymous mutation (global)
Non-synonymous mutation (local)
d
21,217
Nucleotide positions (WA-1)
25,494
NTD
RBD
F
% of single genomes
Thoracic LN (n = 133 sequences)
D 614 G
0 20 40 60 80 100
Synonymous mutation
Non-synonymous mutation (global)
Non-synonymous mutation (local)
e
21,217
Nucleotide positions (WA-1)
25,494
NTD
RBD
F
% of single genomes
Abdominal Aorta (n = 11 sequences)
Pericardium (n = 5 sequences)
Distal Trachea (n = 17 sequences)
Proximal Trachea (n = 161 sequences)
Dura Mater (n = 2 sequences)
R-Bronchus (n = 214 sequences)
L-Bronchus (n = 263 sequences)
R-Inferior Lobe (n = 10 sequences)
L-Inferior Lobe (n = 326 sequences)
R-Middle Lobe (n = 2 sequences)
L-Superior Lobe (n = 4 sequences)
R-Superior Lobe (n = 116 sequences)
Minor Salivary Gland (n = 288 sequences)
Thoracic Aorta (n = 28 sequences)
L 5 F
del F 140
D 178 N
P 295 S
D 614 G
P 621 S
0 20 40 60 80 100
Synonymous mutation
Non-synonymous mutation (global)
Non-synonymous mutation (local)
f
21,217
Nucleotide positions (WA-1)
25,494
NTD
RBD
F
% of single genomes
Hypothalamus (n = 48 sequences)
L-Inferior Lobe (n = 13 sequences)
R-Superior Lobe (n = 18 sequences)
Thalamus (n = 442 sequences)
D 80 F
D 614 G
P 681 H
G 1219 V
0 20 40 60 80 100
Synonymous mutation
Non-synonymous mutation (global)
Non-synonymous mutation (local)

Extended Data Figure 3: **Analysis of SARS-CoV-2 genetic diversity across body compartments in patients**. (a) P18, (b) P19, (c) P27, (d) P33, (e) P36, (f) P38. Haplotype diagrams (left) show SARS-CoV-2 spike single genome sequences detected in multiple organs. Spike NH2-terminal domain (NTD), receptor-binding domain (RBD), and furin cleavage site (F) regions are shaded grey, and remaining regions of the spike are shaded white. Ticks with different colors indicate mutations relative to the WA-1 reference sequence; green indicates non-synonymous differences from WA-1 detected in all sequences in the individual; blue indicates synonymous mutations detected variably within the individual, and pink indicates non-synonymous mutations detected variably within the individual. Bar graphs (right) show the percentage of all single genome sequences in the sample matching each haplotype.

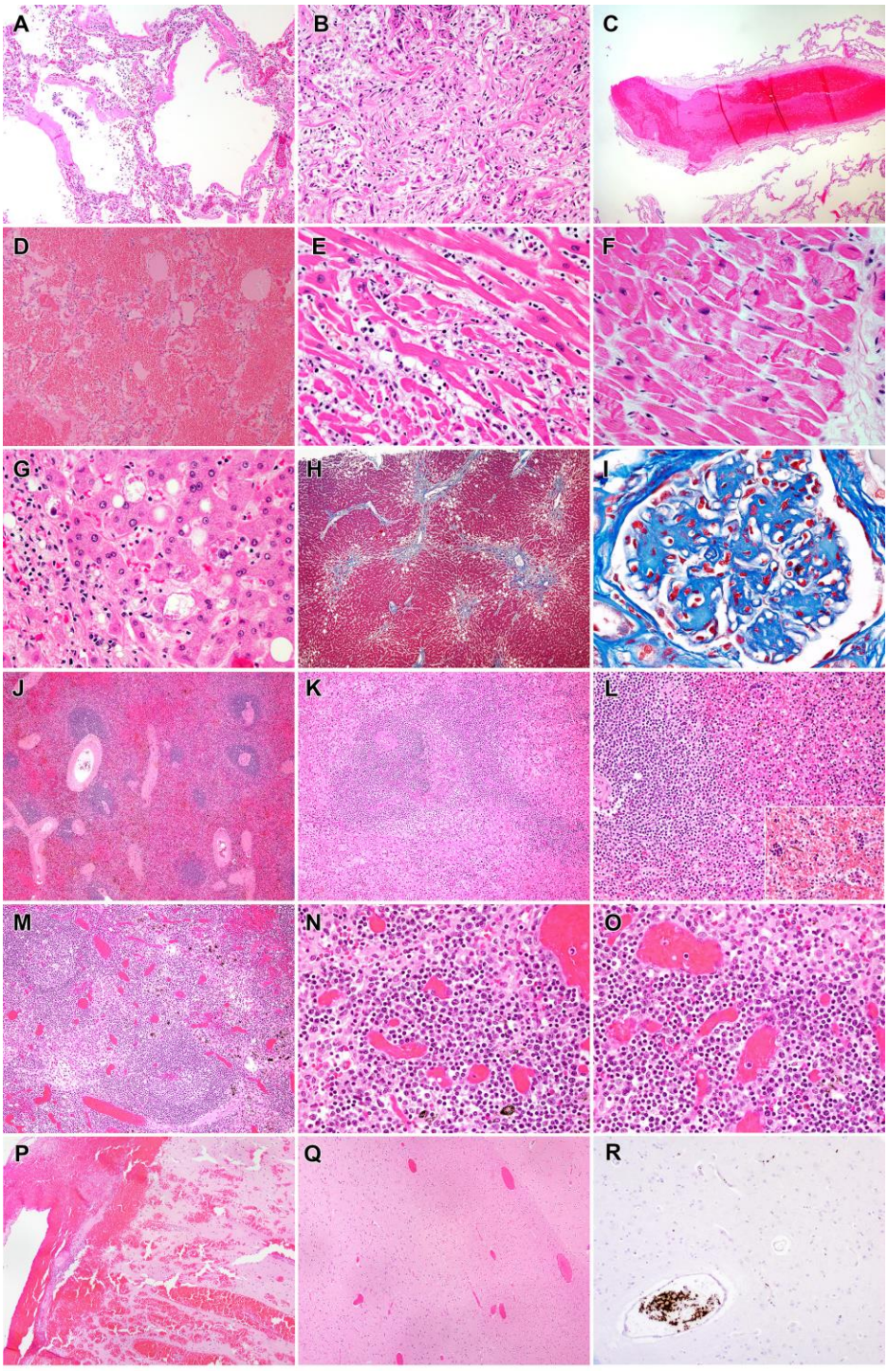

Extended Data Fig. 4 **Representative findings in patients in the COVID-19 cohort**. A. Lung, Subject P22. Exudative phase diffuse alveolar damage with hyaline membranes and mild interstitial inflammation (H&E, 100x). B. Lung, Subject P26. Proliferative phase diffuse alveolar

damage and sparse inflammation. (H&E, 200x). C. Lung, Subject P22. Organizing thrombus in medium sized pulmonary artery. (H&E, 40x). D. Lung, Subject P28. Diffuse pulmonary hemorrhage. (H&E, 100x). E. Heart, Subject P3. Active lymphocytic myocarditis with cardiomyocyte necrosis. (H&E, 400x). F. Heart, Subject P38. Microscopic focus of bland myocardial contraction band necrosis. (H&E, 400x). G. Liver, Subject P41. Steatohepatitis with mild steatosis and scattered ballooned hepatocytes. (H&E, 400x), H. Liver, Subject P41. Focal bridging fibrosis involving central hepatic veins. (Masson trichrome, 40x). I. Kidney, Subject P16. Nodular glomerulosclerosis. (Masson trichrome, 600x). J. Spleen, Subject P16. Preservation of white pulp and congestion (H&E, 40x) K. Spleen, Subject P14. Lymphoid depletion of white pulp with proteinaceous material and red pulp congestion. (H&E, 100x) L. Spleen, Subject P34. Relative preservation of white pulp with extramedullary hematopoiesis (inset) in red pulp (H&E, 200x) M. Lymph node, Subject P25. Follicular hyperplasia with well-defined follicles. (H&E,) N. Lymph node, Subject P25. Marked plasmacytosis in the medullary cord. (H&E, 400x) O. Lymph node, Subject P25. Marked plasmacytosis and sinus histiocytosis. (H&E, 400x) P. Brain, Subject P35, Focal subarachnoid and intraparenchymal hemorrhage. (H&E, 40x) Q. Brain, Subject P44, Vascular congestion. (H&E, 40x) R. Brain, Subject P43, Intravascular platelet aggregates. (anti-CD61 stain, 100x)

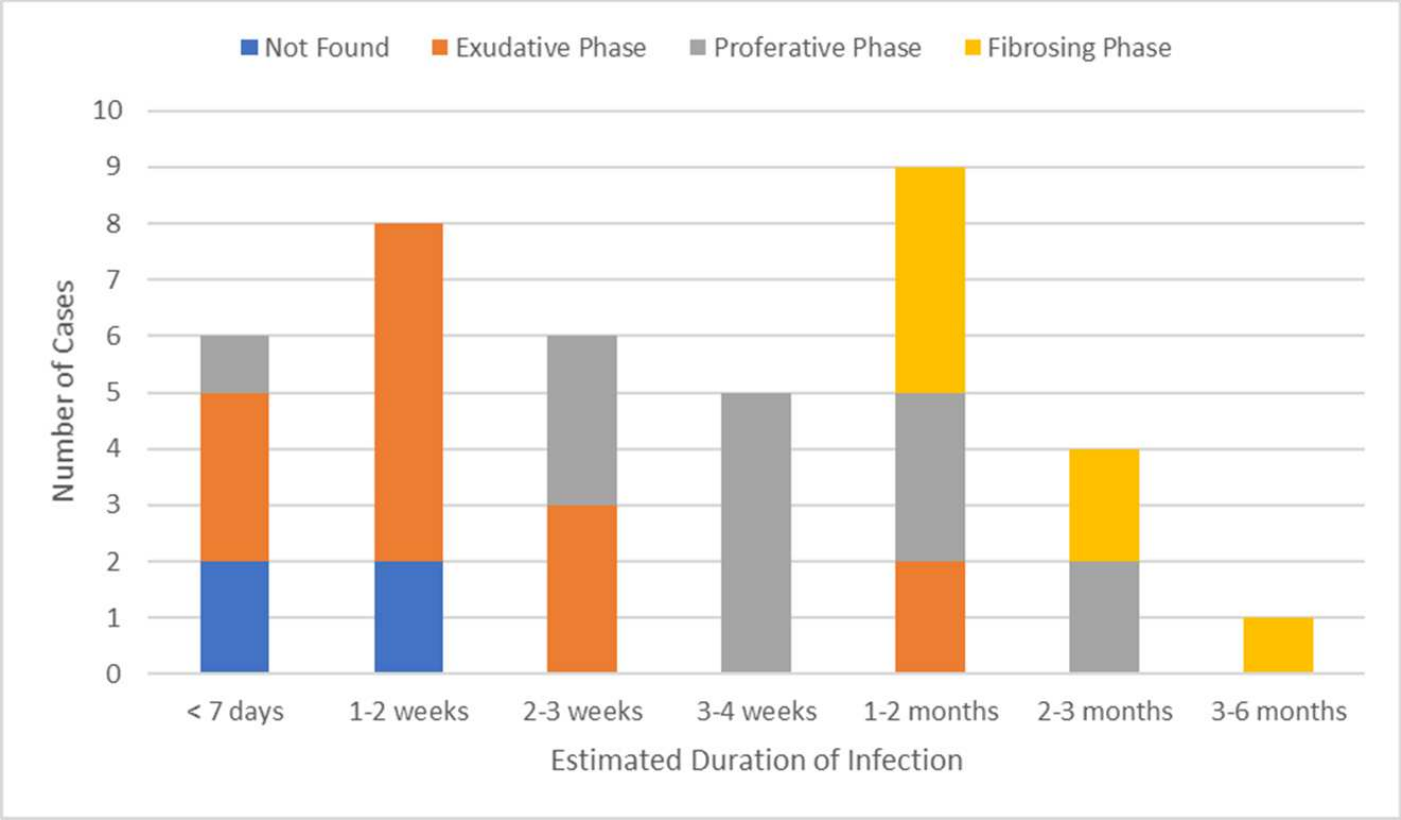

Extended Data Fig. 5 **Temporal association of diffuse alveolar damage in patients dying from COVID-19.** Number of autopsy cases with stages of diffuse alveolar damage via histopathologic analysis by duration of illness. Early time points mainly show the initial exudative phase of diffuse alveolar damage, while patients dying after prolonged illness are more likely to show organizing or fibrosing stages.

a

Age (years)	(n=44)
Mean (Min, Max)	59.2 (6, 91)
Age by group (years)	**n (%)**
0-17	1 (2.3)
18-24	1 (2.3)
25-34	2 (4.5)
35-44	6 (13.6)
45-54	4 (9.1)
55-64	11 (25.0)
65-74	11 (25.0)
75-84	5 (11.4)
≥85	3 (6.8)
Sex	
Male	30 (68.2)
Female	13 (29.5)
Intersex	1 (2.3)
Race/Ethnicity	
Non-Hispanic Asian	1 (2.3)
Non-Hispanic Black or African American	18 (40.9)
Non-Hispanic White	18 (40.9)
Hispanic or Latino	7 (15.9)
BMI	
<18.5	2 (4.5)
18.5-24.9	9 (20.5)
25-29.9	10 (22.7)
30-34.9	9 (20.5)
35.0-39.9	6 (13.6)
≥40	8 (18.1)
Comorbidities	
Autoimmune Disease	5 (11.4)
Cancer	7 (15.9)
Cardiovascular Disease	14 (31.8)
Cerebrovascular Disease	4 (9.1)
Chronic Immunosuppression	6 (13.6)
Chronic Respiratory Disease	15 (34.1)
Diabetes Mellitus	14 (31.8)
History of Thromboembolic Event(s)	3 (6.8)
Hypertension	24 (54.5)
Hyperlipidemia	14 (31.8)
Liver Disease	4 (9.1)
Obesity (body mass index ≥30)	23 (52.3)
Renal Disease	8 (18.2)
1+	42 (95.5)
2+	33 (75.0)
3+	29 (65.9)

b

Disease Course Intervals	Mean (Min, Max)
Symptom onset to hospital admission, days	9.4 (-4, 108)
Symptom onset to death, days	35.2 (1, 230)
Days hospitalized	26.4 (0, 188)
Postmortem Interval (hours)	26.2 (10, 67)
Pharmacologic Interventions	**n (%)**
Vasopressors	38 (86.4)
Antibiotics	41 (93.2)
Systemic Steroids	39 (88.6)
Systemic Anticoagulation	34 (77.3)
Paralytics	25 (56.8)
Inhaled Vasodilators	10 (22.7)
Remdesivir	16 (36.4)
Tocilizumab	4 (9.1)
Convalescent Plasma	6 (13.6)
Nonpharmacologic Interventions	
ECMO	10 (22.7)
Renal Replacement Therapy	18 (40.9)
Intubated	36 (81.8)
Tracheostomy	9 (20.5)
Chest Tube(s)	11 (25.0)

Extended Data Table 1 **Autopsy cohort demographics, comorbidities, and clinical intervention summary**. (a) Summary of demographics and known comorbidities for autopsy cases. (b) Summary of illness course and clinical care for autopsy cases. Data compiled from available patient medical records. ECMO/extracorporeal membrane oxygenation.

Patient ID	Sex	Age, years	Duration of illness, days	BMI	Comorbidities	Immediate Cause of death	Highest level of respiratory support	COVID-19 treatment(s)
Patient 1	M	61	25	31.80	DM, HTN, obesity	Bacterial sepsis and fungal pneumonia	Intubation	Systemic steroids, systemic anticoagulation
Patient 2	F	71	14	39.60	HTN, HLD, COPD, breast cancer, cerebrovascular event, Hx DVT/PE, CHF, AF, dementia, obesity, hypothyroidism, anemia, seizure disorder	Acute pyelonephritis with abscess and likely sepsis	Intubation	Systemic steroids
Patient 3	M	26	14	25.80	Asthma	Lymphocytic myocarditis	Intubation, ECMO	Systemic anticoagulation
Patient 4	M	68	18	31.40	HTN, HLD, obesity	DAD	Intubation	Systemic steroids, remdesivir, tocilizumab, convalescent plasma
Patient 5	M	41	42	50.60	Obesity	Fungal pneumonia	Intubation	Systemic steroids, Systemic anticoagulation
Patient 6	M	62	19	45.00	HTN, obesity	Acute bronchopnuemonia	Intubation	Systemic steroids, systemic anticoagulation, inhaled vasodilators
Patient 7	M	60	7	24.30	DM, CML, HTN, AF, CHF, CAD s/p bypass, PVD, CKD, Hx kidney transplant, chronic immunosuppression, HLD, hyperparathyroidism, hypothyroidism, anemia	Acute polymicrobial bronchopneumonia superimposed on DAD	Intubation	Systemic anticoagulation
Patient 8	F	68	24	58.10	HTN, asthma, COPD, cerebrovascular disease, obesity, anemia, chronic fatigue, fibromyalgia	Acute polymicrobial bronchopneumonia superimposed on DAD	Intubation	Systemic steroids, systemic anticoagulation
Patient 9	M	43	66	34.00	Obesity	Pneumonia and sepsis	Intubation, Tracheostomy, ECMO	Systemic steroids, systemic anticoagulation, paralytics, remdesivir, convalescent plasma
Patient 10	F	70	29	35.43	DM, HTN, HLD, CHF, COPD, obesity	Sepsis	Nasal Canula	Remdesivir
Patient 11	M	50	58	36.70	Obesity	Acute pneumonia	Intubation, Tracheostomy, ECMO	Systemic steroids, systemic anticoagulation, tocilizumab
Patient 12	M	61	48	41.80	DM, HTN, HLD, CHF, LV dysfunction, asthma, obesity	DAD, exudative phase	Intubation	Systemic anticoagulation
Patient 13	M	48	82	41.00	Obesity	DAD, organizing phase	Intubation, Tracheostomy, ECMO	Systemic steroids, systemic anticoagulation, tocilizumab, convalescent plasma
Patient 14	M	64	16	30.60	HTN, COPD, obesity	Acute bacterial bronchoneumonia	Intubation	Systemic steroids, systemic anticoagulation
Patient 15	M	65	27	19.70	HLD, sarcoidosis, chronic immunosuppression	Fungal pneumonia and sepsis	Intubation	Systemic steroids, systemic anticoagulation, remdesivir, convalescent plasma
Patient 16	M	87	8	26.90	DM, HTN, HLD, CAD, CHF, ESRD	DAD, exudative phase	AVAPS	Systemic steroids, systemic anticoagulation, convalescent plasma
Patient 17	M	36	14	27.17	Drug abuse	Bilateral bronchopneumonia	Intubation, ECMO	Systemic steroids, systemic anticoagulation
Patient 18	F	79	9	32.60	DM, HTN, COPD, Hx DVT, CAD, cirrhosis, CKD, obesity, anemia, seizure disorder	DAD, exudative phase	Intubation	Systemic steroids
Patient 19	M	43	7	21.90	DM	Sudden cardiac death	Intubation	Systemic steroids, systemic anticoagulation
Patient 20	M	42	99	23.50	DM, HLD	DAD, proliferative and fibrosing phase	Intubation, Tracheostomy, ECMO	Systemic steroids, systemic anticoagulation, convalescent plasma
Patient 21	M	77	12	25.20	DM, HTN, COPD, pulmonary fibrosis, CAD, CHF, CKD, Hx prostate cancer, cerebrovascular disease	DAD, exudative phase	High flow nasal canula, BiPAP	Systemic steroids, systemic anticoagulation
Patient 22	M	64	4	29.90	HTN, HLD	DAD/ARDS	Intubation	Systemic steroids, systemic anticoagulation
Patient 23	M	79	23	28.00		Pulmonary hemorrhage	Intubation	Systemic steroids, systemic anticoagulation
Patient 24	M	59	12	34.20	Hx recurrent aspiration pneumonia, MS, chronic immunosuppression, obesity	Acute pneumonia	BiPAP	Systemic steroids, systemic anticoagulation
Patient 25	F	91	9	16.50	Cardiomyopathy, arrhythmia, dementia, inflammatory polyneuropathy, anemia	DAD, acute phase	None	Systemic steroids, remdesivir
Patient 26	M	48	29	28.20		Cerebral hemorrhage	Intubation, ECMO	Systemic steroids, systemic anticoagulation, remdesivir
Patient 27	Inter-sex	76	1	20.90	Turner Syndrome, aortic stenosis, sick sinus syndrome s/p pacemaker, dementia, hypothyroidism	Bronchopneumonia and DAD, exudative phase	Intubation	Systemic steroids, systemic anticoagulation, remdesivir
Patient 28	F	44	7	30.9	HTN, obesity	Pulmonary thromboembolic disease in the setting of DAD, exudative phase of	None	
Patient 29	M	60	204	24.91	HTN, ILD, cerebrovascular disease, CAD, RA, Hx lung transplant, chronic immunosuppression	Herpetic tracheobronchitis and DAD, s/p bilateral lung transplantation	Intubation, Tracheostomy, ECMO	Systemic steroids, systemic anticoagulation
Patient 30	F	70	15	26.00	HTN, ILD, PH, CHF, CAD, PAD, CKD, ESRD, congenital heart malformation, calciphylaxis	Bacterial pneumonia, SARS-CoV-2 infection	Intubation	Systemic steroids, systemic anticoagulation, remdesivir
Patient 31	M	59	18	26.50	DM, HTN, HLD	Bacterial pneumonia	Intubation, Tracheostomy	Systemic steroids, systemic anticoagulation, remdesivir
Patient 32	F	71	6	31.50	Asthma, COPD, sarcoidosis, cirrhosis, ESRD, Hx endocarditis, obesity, hypothyroidism, seizure disorder, anemia	Right heart failure	BiPAP	Systemic steroids
Patient 33	M	71	76	29.1	HTN, CKD, Hx Lyme disease	Bacterial pneumonia	High flow nasal canula	Systemic steroids, systemic anticoagulation
Patient 34	M	87	36	22.20	HLD, MM, COPD, CKD, seizure disorder, chronic immunosuppression, hypothyroidism	DAD, organizing to fibrosing phase	Intubation	Systemic steroids, remdesivir
Patient 35	F	45	25	63.00	DM, HTN, HLD, COPD, obesity, chronic lower extremetity lymphedema	DAD, organizing phase	Intubation	Systemic steroids, systemic anticoagulation, remdesivir
Patient 36	F	6	4	17.40	Dravet syndrome, SCN1A gene mutation, seizure disorder	Acute cerebral ischemia with tonsillar herniation	Intubation	Systemic steroids, remdesivir
Patient 37	M	63	5	19.80	DM, HTN, Hx femoral artery thrombosis, CHF, CAD, PAD, AF, cardiomyopathy, Hx cardiac tamponade, hepatitis C, abnormal liver function, drug abuse	Bronchopneumonia	Intubation	Systemic steroids, systemic anticoagulation
Patient 38	M	71	13	40.20	HTN, HLD, COPD, prostate cancer, obesity	Bronchopneumonia	Intubation	Systemic steroids, systemic anticoagulation, remdesivir
Patient 39	M	27	31	39.20	Obesity	DAD, organizing to fibrotic phase and multiple pulmonary infarcts	Intubation, Tracheostomy, ECMO	Systemic steroids, systemic anticoagulation, remdesivir
Patient 40	F	68	47	35.11	HTN, uterine cancer, obesity	Sepsis with signs of cardiac dysfunction in the setting of DAD, proliferative and fibrotic phase	Intubation, Tracheostomy	Systemic steroids, systemic anticoagulation, remdesivir
Patient 41	F	75	33	24.94	DM, HTN, HLD, hypothyroidism	DAD, proliferative and fibrotic phase	Intubation	Systemic steroids
Patient 42	M	68	230	36.87	CAD, hepatitis A, liver failure, Hx liver transplant, chronic immunosuppression, obesity	Massive hepatic necrosis, status-post liver transplant	Intubation, Trachesostomy	Systemic steroids, systemic anticoagulation
Patient 43	F	61	18	32.22	DM, HTN, breast cancer, CAD, obesity	DAD, exudative and proliferative phase	Intubation	Systemic steroids, systemic anticoagulation
Patient 44	M	21	65	58.00	Obesity	Bacterial pneumonia superimposed on DAD, fibrosing stage	Intubation, ECMO	Systemic steroids, systemic anticoagulation, remdesivir, tocilizumab

Extended Data Table 2 **Individual case demographics and clinical summary.** Data obtained from available medical records. AF/atrial fibrillation, AVAPS/average volume-assured pressure support, BiPAP/bilevel positive airway pressure, CAD/coronary artery disease, CHF/congestive heart failure, CKD/chronic kidney disease, CML/chronic myeloid leukemia, COPD/chronic obstructive pulmonary disease, DAD/diffuse alveolar damage, DM/diabetes mellitus, DVT/deep vein thrombosis, ECMO/extracorporeal membrane oxygenation, ESRD/end-stage renal disease, HLD/hyperlipidemia, HTN/hypertension, Hx/historical, ILD/interstitial lung disease, LV/left ventricular, MS/multiple sclerosis, PE/pulmonary embolism, PVD/peripheral vascular disease, PH/pulmonary hypertension, s/p/status post.

a

Tissue Category	DOI (days)	Avg. N gene copies/ng RNA (SD)
Respiratory Tract	≤14	9,210.10 (43,179.20)
	15-30	19.67 (77.98)
	≥31	0.65 (2.61)
Cardiovascular	≤14	38.75 (106.08)
	15-30	0.59 (3.43)
	≥31	0.42 (2.51)
Lymphoid	≤14	30.01 (157.86)
	15-30	0.35 (1.28)
	≥31	0.73 (3.83)
Gastrointestinal	≤14	24.68 (99.37)
	15-30	0.87 (4.38)
	≥31	0.24 (2.17)
Renal & Endocrine	≤14	12.76 (59.01)
	15-30	0.03 (0.16)
	≥31	0.04 (0.33)
Reproductive	≤14	0.36 (0.58)
	15-30	1.87 (6.72)
	≥31	0.01 (0.02)
Muscle, Nerve, Adipose, & Skin	≤14	27.50 (101.13)
	15-30	50.65 (284.46)
	≥31	0.54 (3.03)
Ocular	≤14	57.40 (242.40)
	15-30	0.07 (0.24)
	≥31	0.03 (0.12)
Central Nervous System	≤14	32.93 (121.69)
	15-30	2.37 (7.34)
	≥31	0.39 (1.40)

b

Tissue	DOI (days)	ddPCR+ (n, %)	sgRNA+ (n,%)
All Respiratory		**43/44, 97.7**	**23/43, 53.5**
Trachea	≤14	15/17, 88.2	11/15, 73.3
	15-30	11/13, 84.6	1/11, 9.1
	≥31	12/14, 85.7	0/12, 0
	Total	*38/44, 86.4*	*12/38, 31.6*
Bronchus	≤14	15/17, 88.2	11/15, 73.3
	15-30	10/11, 90.9	1/10, 10.0
	≥31	11/13, 84.6	1/11, 9.1
	Total	*36/41, 87.8*	*13/36, 36.1*
Lung	≤14	16/17, 94.1	14/16, 87.5
	15-30	13/13, 100	5/13, 38.5
	≥31	14/14, 100	3/14, 21.4
	Total	*43/44, 97.7*	*22/43, 51.2*
All Cardiovascular		**35/44, 79.5**	**14/35, 40.0**
Myocardium	≤14	14/17, 82.4	8/14, 57.1
	15-30	8/13, 61.5	0/8, 0
	≥31	9/14, 64.3	0/9, 0
	Total	*31/44, 70.5*	*8/31, 25.8*
Pericardium	≤14	15/17, 88.2	7/15, 46.7
	15-30	5/13, 38.5	1/5, 20.0
	≥31	4/13, 30.8	0/4, 0
	Total	*24/43, 55.8*	*8/24, 33.3*
Aorta	≤14	13/14, 92.9	10/13, 76.9
	15-30	6/10, 60.0	1/5*, 20.0
	≥31	5/13, 38.5	1/5, 20.0
	Total	*24/37, 64.9*	*12/23, 52.2*
Vena Cava	≤14	5/5, 100	1/5, 20.0
	15-30	2/5, 40.0	0/2, 0
	≥31	0/2, 0.0	NA
	Total	*7/12, 58.3*	*1/7, 14.3*
All Lymphoid		**38/44, 86.4**	**16/38, 42.1**
LN from Thorax	≤14	15/17, 88.2	11/15, 73.3
	15-30	11/13, 84.6	2/11, 18.2
	≥31	12/13, 92.3	2/12, 16.7
	Total	*38/43, 88.4*	*15/38, 39.5*
LN from Abdomen	≤14	6/11, 54.5	2/6, 33.3
	15-30	4/8, 50	0/4, 0
	≥31	1/5, 20	0/1, 0
	Total	*11/24, 45.8*	*2/11, 18.2*
Spleen	≤14	12/17, 70.6	3/12, 25.0
	15-30	3/13, 23.1	0/3, 0
	≥31	2/14, 14.3	0/2, 0
	Total	*17/44, 38.6*	*3/17, 17.6*
Appendix	≤14	5/13, 38.5	1/5, 20.0
	15-30	2/9, 22.2	0/2, 0
	≥31	3/13, 23.1	1/3, 33.3
	Total	*10/35, 28.6*	*2/10, 20.0*
All Gastrointestinal		**32/44, 72.7**	**10/32, 31.3**
Salivary Glands	≤14	8/11, 72.7	4/8, 50.0
	15-30	5/11, 45.5	0/5, 0
	≥31	3/13, 23.1	1/3, 33.3
	Total	*16/35, 45.7*	*5/16, 31.3*
Tongue	≤14	2/2, 100	2/2, 100
	15-30	3/5, 60.0	2/3, 66.7
	≥31	3/5, 60.0	0/3, 0
	Total	*8/12, 66.7*	*4/8, 50.0*
Small Intestine	≤14	13/17, 76.5	2/13, 15.4
	15-30	7/13, 53.8	1/7, 14.3
	≥31	5/14, 35.7	0/5, 0
	Total	*25/44, 56.8*	*3/25, 12.0*
Colon	≤14	10/17, 58.8	2/10, 20.0
	15-30	4/11, 36.4	0/4, 0
	≥31	2/14, 14.3	0/2, 0
	Total	*16/42, 38.1*	*2/16, 12.5*
Liver	≤14	10/17, 58.8	4/10, 40.0
	15-30	5/13, 38.5	0/5, 0
	≥31	3/14, 21.4	0/2*, 0
	Total	*18/44, 40.9*	*4/17, 23.5*
All Renal & Endocrine		**28/44, 63.6**	**10/28, 35.7**
Kidney	≤14	12/17, 70.6	4/12, 33.3
	15-30	5/13, 38.5	0/5, 0
	≥31	3/14, 21.4	1/3, 33.3
	Total	*20/44, 45.5*	*5/20, 25.0*
Adrenal Gland	≤14	12/16, 75.0	5/12, 41.7
	15-30	4/13, 30.8	0/4, 0
	≥31	5/14, 35.7	0/5, 0
	Total	*21/43, 48.8*	*5/21, 23.8*
Thyroid	≤14	10/16, 62.5	7/10, 70.0
	15-30	4/12, 33.3	0/4, 0
	≥31	3/13, 23.1	0/3, 0
	Total	*17/41, 41.5*	*7/17, 41.2*
Pancreas	≤14	11/17, 64.7	3/11, 27.3
	15-30	3/12, 25.0	0/3, 0
	≥31	2/14, 14.3	0/2, 0
	Total	*16/43, 37.2*	*3/16, 18.8*

Tissue	DOI (days)	ddPCR+ (n, %)	sgRNA+ (n,%)
All Reproductive		**17/40, 42.5**	**2/17, 11.8**
Ovary	≤14	3/5, 60.0	0/3, 0
	15-30	0/3, 0	NA
	≥31	NA	NA
	Total	*3/8, 37.5*	*0/3, 0*
Uterus	≤14	1/1, 100	0/1, 0
	15-30	2/2, 100	1/2, 50.0
	≥31	NA	NA
	Total	*3/3, 100*	*1/3, 33.3*
Testis	≤14	7/10, 70.0	1/7, 14.3
	15-30	1/8, 12.5	0/1, 0
	≥31	3/12, 25.0	0/3, 0
	Total	*11/30, 36.7*	*1/11, 9.1*
Muscle, Skin, & Peripheral Nerves		**30/44, 68.2**	**9/30, 30.0**
Skeletal Muscle	≤14	12/17, 70.6	5/12, 41.7
	15-30	7/13, 53.8	1/7, 14.3
	≥31	3/14, 21.4	0/3, 0
	Total	*22/44, 50*	*6/22, 27.3*
Skin	≤14	3/3, 100	1/3, 33.3
	15-30	1/1, 100	0/1, 0
	≥31	1/7, 14.3	0/1, 0
	Total	*5/11, 45.5*	*1/5, 20.0*
Peripheral Nervous System	≤14	13/15, 86.7	5/13, 38.5
	15-30	6/11, 54.5	0/6, 0
	≥31	7/14, 50.0	2/7, 28.6
	Total	*26/40, 65.0*	*8/26, 30.8*
All Ocular		**22/38, 57.9**	**7/21*, 33.3**
Ocular Tissue	≤14	9/12, 75.0	6/9, 67.7
	15-30	4/9, 44.4	0/4, 0
	≥31	6/11, 54.5	1/5*, 20.0
	Total	*19/32, 59.4*	*7/18, 38.9*
Ocular Humor	≤14	6/13, 46.2	1/6, 16.7
	15-30	3/11, 27.3	0/3, 0
	≥31	2/10, 20.0	0/1*, 0
	Total	*11/34, 32.4*	*1/10, 10.0*
Optic Nerve	≤14	10/12, 83.3	3/10, 30.0
	15-30	2/6, 33.3	0/2, 0
	≥31	5/11, 45.5	0/5, 0
	Total	*17/29, 58.6*	*3/17, 17.6*
All Central Nervous System		**10/11, 90.9**	**4/10, 40.0**
Cervical Spinal Cord	≤14	2/2, 100	1/2, 50.0
	15-30	1/1, 100	0/1, 0
	≥31	5/6, 83.3	0/5, 0
	Total	*8/9, 88.9*	*1/8, 12.5*
Olfactory Nerve	≤14	2/3, 66.7	1/2, 50.0
	15-30	1/2, 50.0	0/1, 0
	≥31	3/5, 60.0	0/3, 0
	Total	*6/10, 60.0*	*1/6, 16.7*
Basal Ganglia	≤14	1/2, 50.0	0/1, 0
	15-30	1/2, 50.0	0/1, 0
	≥31	3/4, 75.0	0/3, 0
	Total	*5/8, 62.5*	*0/5, 0*
Cerebral Cortex	≤14	3/3, 100	1/3, 33.3
	15-30	1/2, 50.0	1/1, 100
	≥31	5/6, 83.3	0/5, 0
	Total	*9/11, 81.8*	*2/9, 22.2*
Brainstem	≤14	3/3, 100	1/3, 33.3
	15-30	1/2, 50.0	1/1, 100
	≥31	4/5, 80.0	0/4, 0
	Total	*8/10, 80.0*	*2/8, 25.0*
Cerebellum	≤14	2/3, 66.7	0/2, 0
	15-30	1/2, 50.0	0/1, 0
	≥31	6/6, 100	0/6, 0
	Total	*9/11, 81.8*	*0/9, 0*
Thalamus	≤14	2/2, 100	1/2, 50.0
	15-30	1/2, 50.0	0/1, 0
	≥31	5/6, 83.3	0/5, 0
	Total	*8/10, 80.0*	*1/8, 12.5*
Hypothalamus	≤14	2/2, 100	1/2, 50.0
	15-30	1/1, 100	0/1, 0
	≥31	4/4, 100	0/4, 0
	Total	*7/7, 100*	*1/7, 14.3*
Corpus Callosum	≤14	2/2, 100	0/2, 0
	15-30	1/1, 100	0/1, 0
	≥31	4/4, 100	0/4, 0
	Total	*7/7, 100*	*0/7, 0*
CNS Vasculature	≤14	2/2, 100	0/2, 0
	15-30	1/2, 50	0/1, 0
	≥31	3/5, 60	0/3, 0
	Total	*6/9, 66.7*	*0/6, 0*
Dura Mater	≤14	3/3, 100	2/3, 66.7
	15-30	0/1, 0	NA
	≥31	0/5, 0	NA
	Total	*3/9, 33.3*	*2/3, 66.7*

Extended Data Table 3 **Summary of SARS-CoV-2 RNA and sgRNA by tissue category over time**. (a) Summary of the average nucleocapsid gene copies/ng RNA across cases by tissue category and duration of illness (days). (b) Summary of the number and percentage of cases with SARS-CoV-2 RNA detected via droplet digital (dd)PCR by tissue category for all cases and by tissue and duration of illness (days). The number and percentage of tissues positive for ddPCR that were additionally positive for subgenomic (sg)RNA PCR is listed in the right most column. *A tissue positive via ddPCR was not tested via sgRNA PCR. CNS/central nervous system, LN/lymph node.

Cell Type	Locations
Bile duct epithelium	Liver
Chondrocytes	Bronchial cartilage rings
Collecting duct epithelium	Kidney
Distal tubule epithelium	Kidney
Endocrine cells of adrenal	Adrenal gland
Endocrine cells of thyroid	Thyroid
Endothelium	Vasculature, all
Ependyma	Brain
Exocrine cells of pancreas	Pancreas
Fibroblast-like cells	Pericardium, heart, trachea, bronchus
Germ cells	Testis
Glandular epithelum	Uterus
Glia	Brain, all locations
Hepatocytes	Liver
Hyaline Membrane	Lung
Interstitial cells of endometrium	Uterus
Intimal cells	Aorta
Kupffer cells	Liver
Leydig cells	Testis
Mononuclear leukocytes	Lung, spleen, lymph nodes, lymphoid aggregates of GI
Mucosal epithelium	Small intestine, colon
Mucus secreting epithelium, salivary type	Salivary glands, trachea, bronchus
Myocytes, Cardiac	Heart
Myocytes, Striated	Psoas muscle
Myocytes, Smooth	Uterus, GI
Neurons	Brain, all locations
Parietal cells	Kidney, Bowman's capsule
Pneumocytes, type I & II	Lung
Purkinje cell	Cerebellum
Schwann cells	Nerves, all
Sertoli cells	Testis
Stratified epithelium (& basal layer)	Trachea, esophagus
Stromal cells	Pericardium, uterus, ovary
Vascular smooth muscle	Arteries, all

Extended Data Table 4 **SARS-CoV-2 cellular tropism**. Summary of cell types that were identified as SARS-CoV-2 positive by ISH, and the corresponding anatomic sites in which this was observed.

Cause of Death	N = 44
Death with (but not from) COVID-19	5 (11%)
Death from COVID-19 or complications	39 (89%)
Pulmonary Findings[1]	**N (%) or Median (IQR)**
Left Lung Weight (g)[2]	795 (327)
Right Lung Weight (g)[2]	820 (365)
Combined Lung Weight (g)	1600 (528)
Diffuse Alveolar Damage	
Exudative	14 (32%)
Proliferate	15 (34%)
Fibrosing	7 (16%)
Not Found	8 (18%)
Acute Pneumonia	27 (61%)
Pulmonary Edema	30 (68%)
Pulmonary Hemorrhage (at least focal)	14 (32%)
Pulmonary Thromboembolism, Infarction	10 (23%)
Emphysematous changes (underlying COPD)	12 (27%)
Cardiac Findings	
Heart Weight (g)	500 (175)
Myocardial Infiltrate	4 (9%)
Focal infiltrate without myocyte necrosis	3 (7%)
Diffuse lymphocytic myocarditis	1 (2%)
Myocardial Ischemic Necrosis	
Remote, fibrotic	5 (11%)
Acute microscopic ischemia	4 (9%)
Coronary Artery Disease with ≥ 50% in at least 1 artery	16 (36%)
Renal Findings	
Left Kidney Weight (g)[4]	180 (107)
Right Kidney Weight (g)[4]	168 (79)
Changes consistent with Acute Kidney Injury	17 (39%)
Changes consistent with Diabetic glomerulopathy	10 (23%)
Splenic Findings	
Splenic Weight (g)	235 (215)
Follicular hyperplasia	15 (34%)
Lymphodepletion	
Present	8 (18%)
Some, Partial Preservation	34 (77%)
No Lymphodepletion	2 (5%)
Red Pulp Congestion	35 (80%)
Infarction	2 (5%)

Lymph Node Findings[5]	N (%) or Median (IQR)
Lymphodepletion	
Present	5 (12%)
Some, Partial Preservation	4 (10%)
No Lymphodepletion	31 (78%)
Follicular Hyperplasia	
Present	22 (55%)
Present, regressed	2 (5%)
Paracortical Hyperplasia	32 (80%)
Plasmacytosis	19 (48%)
Plasmablasts noted	4 (10%)
Hepatic Findings[3]	
Liver Weight (g)[4]	1670 (900)
Hepatic necrosis	
None	30 (70%)
Zonal	12 (28%)
% Zonal Necrosis	30% (40%)
Massive	1 (2%)
Steatosis	
None to Minimal	24 (56%)
Mild	14 (33%)
Moderate	5 (12%)
Steatohepatitis	5 (12%)
Portal Inflammation	
None to Minimal	16 (37%)
Mild	23 (53%)
Moderate	4 (9%)
Fibrosis	
None	27 (63%)
Periportal or perisinusoidal	6 (14%)
Periportal and perisinusoidal	1 (2%)
Bridging fibrosis	6 (14%)
Cirrhosis	3 (7%)
Central Nervous System Findings (N=11)	
Brain Weight (g)	1350 (230)
Hypoxic/Ischemic Injury (focal or diffuse)	5 (45%)
Vascular congestion	5 (45%)
Focal (microscopic) hemorrhage	2 (18%)
No pathological findings	3 (27%)

Extended Data Table 5 **Histopathologic findings of COVID-19 autopsy cases**. Summary of histopathologic findings across organ system across 44 autopsy cases. Central nervous system findings are reported for the 11 cases in which consent for sampling was obtained. [1]Includes one

883 case in which the COVID lungs were transplanted and data from explanted lungs used in table.

884 [2]Individual lung weights were missing in 4 cases. [3]Findings missing on 1 case due to extreme

885 autolysis. [4]Weight missing on one case. [5]Lymph node findings missing in 4 cases

Supplementary Files

This is a list of supplementary files associated with this preprint. Click to download.

- SupplementaryData1.xlsx
- SupplementaryData2.xlsx